School of Geography and the Environment

Dissertation

Essay Title: How does the Bilybara High impact regional rainfall and temperature, both in the present day and in future projections?

Word count: 11,976

Abstract

In Australia, extreme drought and heatwave events have been severely problematic in the past and are predicted to increase in frequency and intensity in the future. The Bilybara High is one regional circulation feature over Australia that could be particularly important for these future climate changes as it is known to influence mean rainfall and temperature. This study will investigate the Bilybara High, both through daily ERA5 reanalysis data and daily model data, to determine the relationships between the High and rainfall and temperature.

Results show that on days experiencing a strong Bilybara High compared to days with no High, rainfall can decrease by as much as 16mm per day over north-west Australia, and temperature can increase by as much as 7°C over large areas of western Australia. Moreover, when the High is strong, there is a 38% increase in the frequency of days with very low rainfall, a 37% increase in the frequency of high temperature days, and a 34% reduction in the frequency of the number of days with heavy rainfall, compared to when there is no High.

After establishing the relationships between the High and rainfall and temperature, consideration is given to how the Bilybara High and its relationships with rainfall and temperature are represented in historical (1980-2005) and future (2075-2100) model simulations from phase 5 of the Coupled Model Intercomparison Project. In the historical simulations, thirteen of the twenty models underestimate the strength of the High, and seven overestimate it compared to ERA5. Comparing historical model simulations to future simulations, eight models show the High is stronger in the future, and twelve show the High is weaker in the future. Historical simulations generally capture the relationships between the High and mean and extreme rainfall and temperature in models well. When discovering whether similar relationships exist in future simulations, we observe generally similar patterns, with some variations in the relative magnitude of change and spatial extent. A key difference between historical and future simulations is that, when comparing strong High days to no High days, future simulations have a larger spatial extent of maximum mean temperature increase. The spatial extent covers approximately the whole of the Australian landmass (over 7.5 million km^2) in the future compared to mainly the north and west of Australia (approximately 4-5 million km^2) in historical simulations. This relates to the larger spatial extent of the High in future simulations. Additionally, when comparing strong High days to no High days, we find the maximum relative frequency of extreme high temperature days increases from 48% to 62% from historical to future model simulations. Similarly, the relative frequency of extreme heavy rainfall days decreases from -60% to -71%. Therefore, the results show an increase in extreme weather events in the future.

The final section explores whether intermodel variability in future projections of the High could help to explain the spread of future projected rainfall and temperature. The key result shows that there is a strong negative correlation ($r=-0.660$, $p<0.01$, $n=20$) between the variability in the model representations of the change in the strength of the High and variability in the change in rainfall among models. This ultimately means that the evolution of the Bilybara High is likely to be significant in determining rainfall in the future.

The results of this study clearly show that the Bilybara High plays a key role in rainfall and temperature patterns across Australia, and therefore is likely to be an important driver of extreme drought and heatwave events in the future. This information advances the science of local circulation features and can be important for governments and policymakers who must prepare and adapt for future regional climate changes in Australia.

Acknowledgments

I would like to thank my supervisor for his invaluable support and guidance throughout the project, as well as his patience during a testing summer of COVID-19 and lockdowns.

I would like to thank Dr Sebastian Engelstaedter from the School of Geography and the Environment for the coding classes he taught, without which this dissertation would not have been possible.

I would like to thank all those from the School of Geography and the Environment who gave climate lectures in year 1 of the Geography course. The lectures were my initial inspiration for a climate dissertation.

Finally, my thanks go to those who contributed to the Coupled Model Intercomparison Project Phase 5; their work underpins the results found in this dissertation.

Table of Contents

Section 1: Introduction

1.1 Overview of research

Australia has an extremely complex and variable climate, with variability in temperature and rainfall influenced by climate processes operating on regional to global scales (Risbey et al., 2009; Wang et al., 2017; Arriagada et al., 2019). Often, during the austral summer, the country experiences very high temperatures and low rainfall, which creates drought and heatwave prone conditions (Bureau of Meteorology, 2008a). This can have serious environmental, social and economic effects (e.g., Matusick et al., 2016; Edwards et al., 2018; Hopkins et al., 2018; Arriagada et al., 2019; Lim et al., 2019; Kirono et al., 2020). For example, drought and heatwave events can cause extensive destruction to natural ecosystems and increase the risk of wildfires (Zhao and Dai, 2015; Virgilio et al., 2019). Recent extensive wildfires, caused by such events, have resulted in serious impacts including human injuries, deaths, and broad-scale environmental damage (Worthy and Wasson, 2004; Sharples et al., 2016; Dowdy et al., 2019). Together this has led to an estimated annual economic cost nearing $8.5 billion (Ashe et al., 2009), including $4.4 billion for one event in 2009 alone (Teague et al., 2010). Given the high cost to society, it is important to fully understand the climatic drivers of extreme drought and heatwaves, and how they might change in the future.

Large-scale circulation anomalies induced by global and regional sea-surface temperature (SST) variability can cause drought and heatwaves over Australia. For example, the Southern Annular Mode (SAM) is a main driver of Australian climate variability, with a positive phase in autumn and winter seasons being associated with dry conditions (Marshall, 2003). Previous winters have been subject to a strong positive SAM, ultimately a central factor to the ‘Big Dry’ seen in southern Australia from 1997-2009 (Gergis et al., 2012). Projections over Australia suggest that droughts and heatwaves will become more common in the future (IPCC, 2012; Cook et al., 2014; Arriagada et al., 2019). However, there is a large range of model projections, with CMIP5 models ranging from a 40% increase to a 40% decrease in monsoonal rainfall due to model biases in SSTs (Brown et al., 2016). We do not have a full grasp of the processes that drive the uncertainty in projections between models, but this is important to know if we are to judge the plausibility of projections and potentially constrain the range of possible futures (Knutti and Sedlacek, 2013).

One way to understand how climate change will play out in the future over Australia is to investigate specific features of the regional circulation known to be important for regional rainfall and temperatures. Elsewhere in the subtropics, this has been successful in explaining variability in rainfall projections. For example, research in southern Africa has shown that projections of drying

are linked with changes to an important convergence line known as the Congo Air Boundary (Howard and Washington, 2020). In Australia, one feature that could be particularly important for constraining future changes is the Bilybara High, a mid-level anticyclone that occurs over north-western Australia. Based on coarse resolution (2.5°x2.5°) NCEP reanalysis data using monthly mean values, Reason (2016, 2018) shows that the Bilybara High plays a key role in temperature and rainfall patterns across large parts of Australia on monthly timescales, whereby increases in the strength of the High result in increased temperatures and decreased rainfall.

Despite its importance, the Bilybara High has not been investigated thoroughly, and not in high-resolution reanalysis. We do not yet know how it affects extreme rainfall and temperature. We also do not know how well climate models reproduce the High, how the High is projected to change in the future, and whether such change is associated with rainfall and temperature changes. Hence, this study will address the following central question: How does the Bilybara High impact regional precipitation and temperature, both in the present day and in future projections. To answer this question, this dissertation is divided into four research questions:

1) How does the Bilybara High impact rainfall and temperature in the high-resolution ERA5 reanalysis data?
2) How is the Bilybara High and its relationships with rainfall and temperature represented in historical (1980-2005) CMIP5 simulations?
3) How is the Bilybara High and its relationships with rainfall and temperature represented in future (2075-2100) CMIP5 simulations?
4) How does the Bilybara High change in the future compared to now, and how does that relate to changes in rainfall and temperature?

The remainder of Section 1 provides background to the research questions. An overview of the Bilybara High is given in Section 1.2. Section 1.3 summarises CMIP5 models over Australia. Section 2 presents the details of the data and methodology used. The results of the study are presented and discussed in Sections 3, 4, 5, and 6, addressing each of the research questions respectively. In Section 7, the main findings are outlined, suggestions are presented for future research, and final remarks are made.

1.2 Introduction to the Bilybara High

Figure 1 outlines the main drivers of Australian climate variability. The Indian Ocean Dipole (IOD), Madden-Julian Oscillation (MJO), El Niño Southern Oscillation (ENSO), and Southern Annular

Mode (SAM) have varying effects on rainfall and temperature throughout the year (Power et al., 1999; Meneghini et al., 2007; Marshall, 2014; Lim et al., 2016). For example, literature generally associates the La Niña phase of ENSO with increased rainfall across much of Australia (Risbey et al., 2009). These modes have been thoroughly studied and their impacts are well known. Figure 1 also shows the Bilybara High, a less well-studied part of the regional Australian climate. The Bilybara High is a semi-permanent anticyclone that is present for parts of the year in the mid-troposphere (around 500 hPa) above north-west Australia and is an important component of the austral summer climate (Reason, 2016). The High forms to the southwest of an anticyclone at 200hPa through upper-level divergence over the area of high tropical rainfall (Indonesia) and planetary vorticity advection (Lenters and Cook, 1997; Reason, 2018).

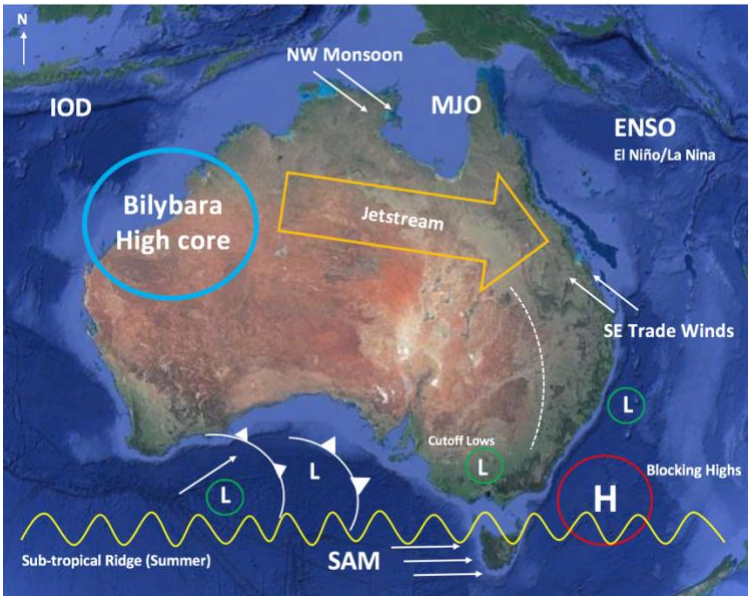

Figure 1 – A schematic presenting the key regional climate features and modes of climate variability across Australia. Adapted from Climate Change in Australia (2016).

The Bilybara High was first identified by Lenters and Cook (1997) as one of three high-pressure systems (alongside the Bolivian High in South America and the Botswana High in Southern Africa) seen across the Southern Hemisphere in response to regions of high precipitation to their northeast (Figure 2). The paper identified these climate features and suggested a mechanism for their formation. This mechanism was of local overturning circulations in response to condensational heating and suggests that a convective core over high precipitation to the northeast sets up a local overturning circulation, which causes outflow at the upper atmospheric levels and subsidence over the core region of the High. Above the core region a thermal low forms because of intense surface heating and dry air not rising through the atmosphere due to an absence of water vapour. The subsidence from the overturning circulation meeting the air being pushed up by the thermal low results in an excess of air at 500hPa which creates the High. This overturning circulation can be shown in Figure 3. By

comparing the vertical velocities of days with differing High strengths we can determine the differences in overturning circulation on strong and no High days. Figure 3 shows that upward motion in lower atmospheric levels above the core region of the High is much stronger for strong High days, with a difference in vertical velocity of -0.027 Pa/s between strong and no High days. This suggests that the critical factor determining the strength of the High is the presence of the heat low from approximately 950-450hPa at 19°-20°S. Interestingly, Figure 3 also shows that the subsidence from the upper atmosphere at the latitude of the High is weaker during strong High days - vertical velocity decreases from 0.027 Pa/s on no High days to 0.018 Pa/s on strong High days. In general, Figure 3 shows the local overturning circulation associated with the formation of the High, which corroborates the theory of Lenters and Cook (1997).

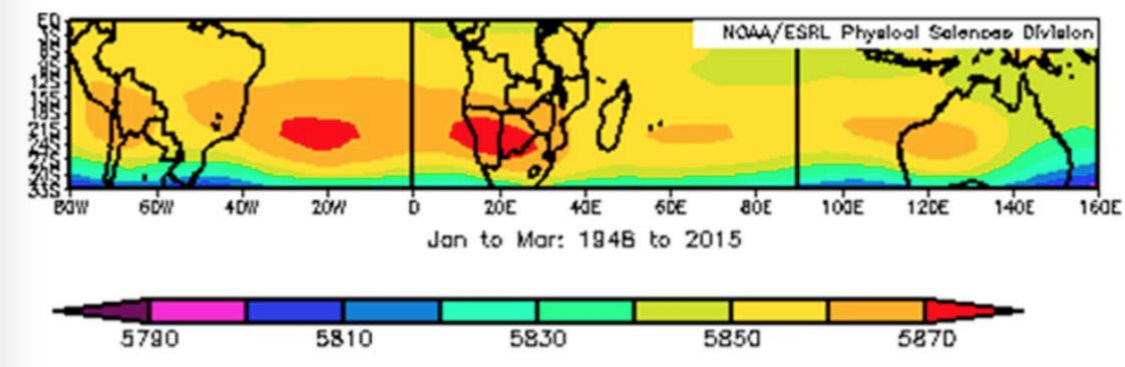

Figure 2 – An NCEP reanalysis mean 500hPa geopotential height field in JFM showing a ridge of high pressure extending across the Southern Hemisphere with anticyclones located over Bolivia, Botswana, and Australia, as well as the south Atlantic (Reason, 2016).

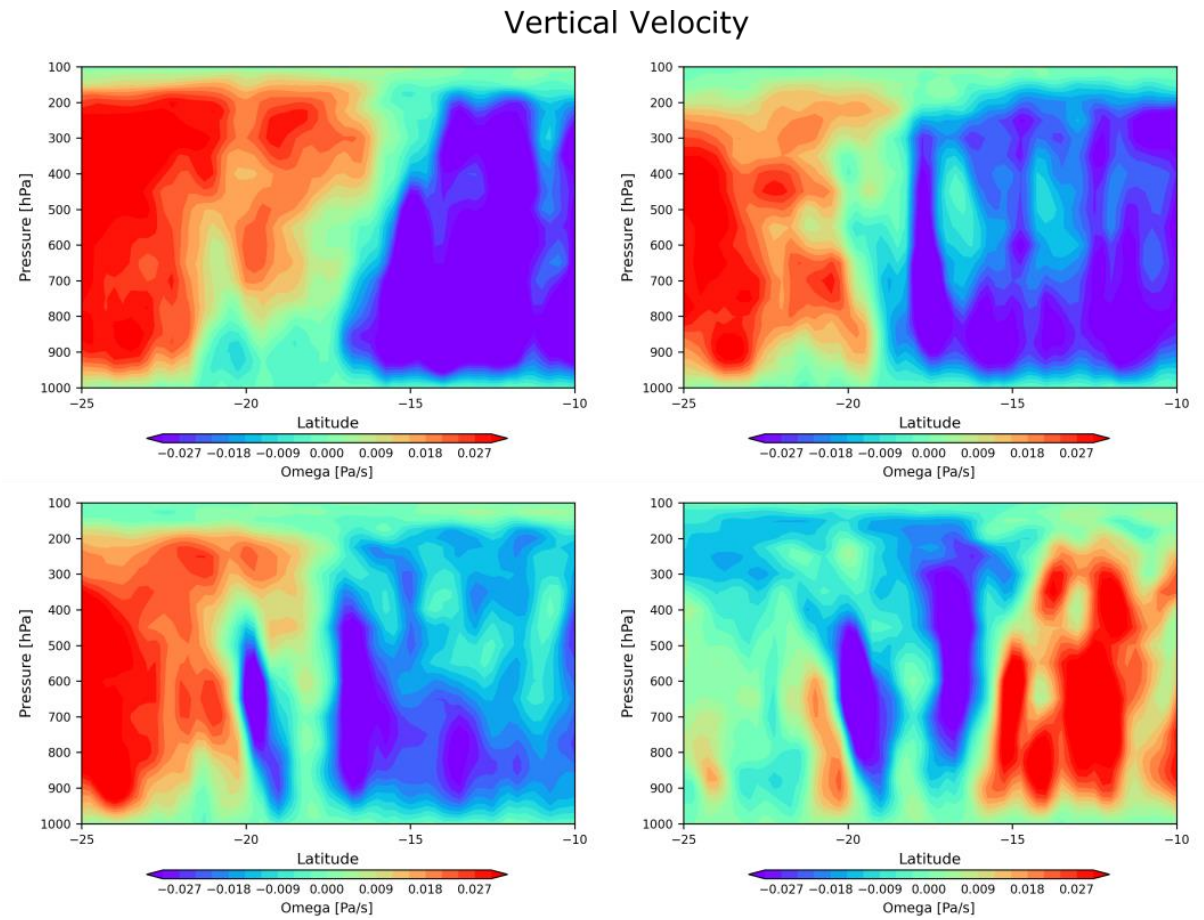

Figure 3 –A cross-section of vertical velocity over the latitudes of 10°-25°S to show the local overturning circulation system that forms the Bilybara High. This plot is produced by averaging daily ERA5 omega (Pa/s) values in March over the years 2000-2018. The plots are composites of no (top left), weak (top right) and strong (bottom left) High days, and an anomaly of strong-minus-no High days (bottom right). For details of ERA5 data used and method to select strong/weak/no High days see Section 2.

The annual cycles of all three Highs follow similar patterns, with the Bilybara High appearing between August and May. From August the High starts to move southward from around 14°S and gradually increases in magnitude. By January the High is at 23°S, 125°E. In February and March, the core of the High is near 25°S and is at its greatest intensity. From April onwards the High retreats northward and intensity decreases, until May when it is no longer clearly evident (Reason, 2016; Reason, 2018). The annual strength of the Bilybara High can be seen in Figure 4. The Figure clearly shows that the strength of the High is at its maximum between January and March, with March experiencing the largest average geopotential height (GPH) of 5870m. The strength of the High decreases at a fairly constant rate until July, reaching a minimum average GPH of 5815m, before starting to increase again coming into austral spring.

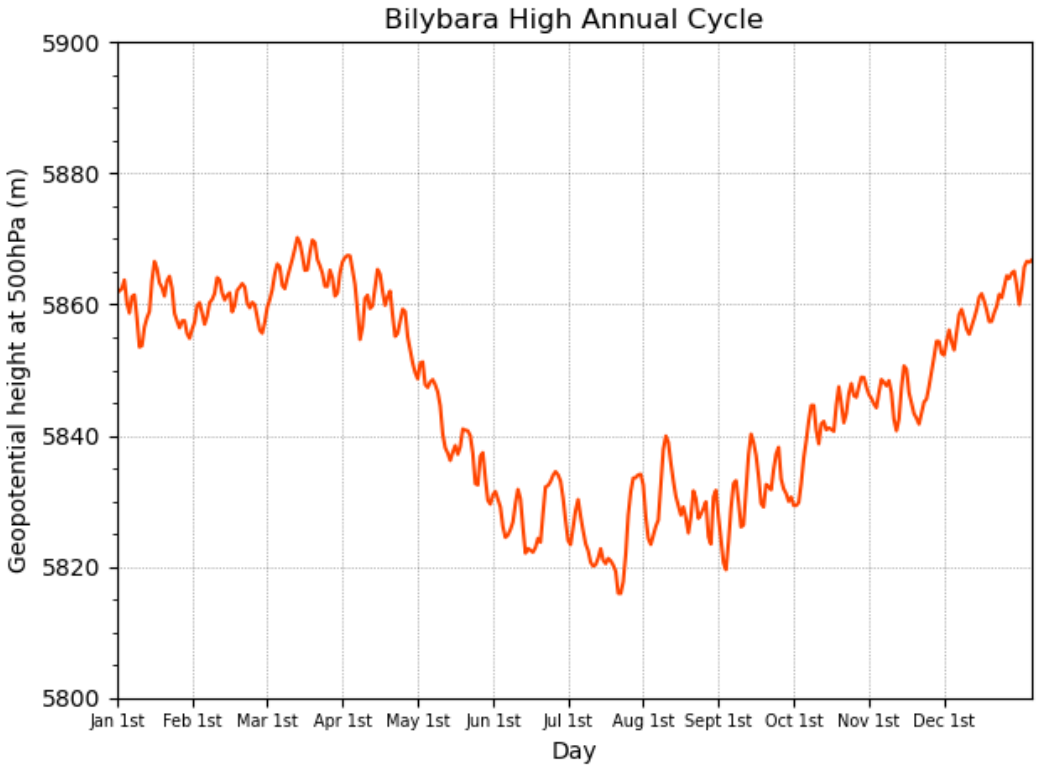

Figure 4 – The annual cycle of the strength of the Bilybara High based on daily ERA5 geopotential height (m) at 500hPa (averaged over 2000-2018). For details of data used see Section 2.

Since the Lenters and Cook paper (1997), the Bolivian and Botswana Highs have been studied further (e.g., Driver and Reason, 2017), however, the Bilybara High has seen little additional research. From the limited literature available, it is evident that the Bilybara High is an important component of rainfall variability over the Australian region on interannual and decadal timescales (Reason, 2018). The strength of the High can vary from year to year: a stronger High is associated with a drier and hotter summer, while a weaker High is associated with a wetter summer (Reason, 2018). This is shown in the correlation between the strength of the High and rainfall which ranges from -0.3 to -0.6 over central and northern Australia (Reason, 2018). Reason (2018) determined that there are several ENSO neutral years when variations in the High have a direct impact on regional precipitation and temperature. This highlights the significance of the High within the climatic system as it shows the feature can act independently of other modes of variability. Fundamentally, when the High is stronger than average, weaker monsoonal north-westerlies are present over the Timor Sea and northern Australia with reduced mid-level uplift, causing a suppression of rainfall (Reason, 2018). These drier conditions are often emphasised by increases in maximum temperatures and the frequency of days with temperatures exceeding the 90th percentile (Reason, 2018). Correlations between the strength of the High and maximum surface air temperature range from 0.3-0.6 across large areas of central and northern Australia and correlations between the strength of the High and the number of days exceeding the 90th percentile in surface air temperature range from 0.3-0.5 across central Australia

(Reason, 2018). The results of Reason (2018) are based on NCEP reanalysis data with the relatively low resolution of 2.5°x2.5°.

1.3 Simulation of Australian climate in CMIP5 models

The global climate can be studied using models. These models are based upon scientific theory, whereby thermodynamic laws and equations of motion are applied to three-dimensional grid boxes that divide up the Earth's surface, oceans, and atmosphere. Such models take into consideration a large number of highly complex factors, with the most up-to-date models including carbon cycles, dynamic vegetation, and ocean circulations (James et al., 2015). The raw data produced from these models covers many climatological variables for land-based, atmospheric, and oceanic study. Essentially, models provide the best available way of studying the climate and making projections about the future (Tyson and Preston-Whyte, 2000).

Models are an important way of studying the climate system on global and regional scales. The Bilybara High plays a key role in rainfall and temperature variability over the Australia region, and thus it is necessary to assess how well models simulate the High. These models can then be used for future predictions of the High and its impacts on rainfall and temperature, ultimately aiding the implementation of any future policymaking.

1.3.1 Background to CMIP5 models

This study will be using a range of Coupled Model Intercomparison Project Phase 5 (CMIP5) models to assess the High and its relationship with temperature and rainfall for the periods of 1980-2005 and 2075-2100. CMIP5, completed from 2010-2014, is a set of thirty-five climate model experiments aiming to improve the understanding of the climate system and provide assessments for future climate change by forcing General Circulation Models with anthropogenic emissions of greenhouse gases (IPCC, 2013). Ensembles of these models are used by the Intergovernmental Panel on Climate Change (IPCC) to predict the future impacts of anthropogenic climate change for potential economic and political pathways (Taylor et al., 2012). For this study, the RCP8.5 forcing has been chosen for future models. RCP8.5 is a pathway that approximately results in a radiative forcing of 8.5 W m^{-2} at 2100 relative to pre-industrial conditions (IPCC, 2013).

1.3.2 Representation of present-day Australian climate in CMIP5 models

CMIP5 simulations have some considerable biases in Australian climate simulation, including those associated with mean temperatures, rainfall, and the Australian monsoon (Irving et al., 2012). Regarding temperature, the models generally underestimate observed mean temperature trends and vary in outputs for spatial patterns of heatwaves but can reproduce the phase and strength of the seasonal temperature cycle over Australia (Irving et al., 2012; Gibson et al., 2017). Furthermore, temperature extremes are largely quite well simulated, except maximum extremes are often underestimated and minimum extremes are often overestimated (Alexander and Arblaster, 2017). For precipitation, inter-model differences occur. There are generally underestimates or overestimates of precipitation depending on season or location, and models struggle to even agree on the direction of change (Irving et al., 2012; Smith et al., 2012: Moise et al., 2015). For example, the CMIP5 models seem to overestimate rainfall over the Tasman Sea in the winter months, potentially because of models failing to simulate atmospheric blocking (Irving et al., 2012); and ACCESS models tend to simulate light rainfall too frequently and underestimate the intensity of heavy rainfall (Brown et al., 2010). Overall, most CMIP5 models can represent the main features of the Australian climate and reproduce key modes of variability (Moise et al., 2015). However, they show some key faults in simulating finer elements, especially for rainfall.

1.3.3 Future projections of rainfall and temperature over Australia

Future projections of Australian climatology using CMIP5 models contain many discrepancies, especially with regards to rainfall. Model agreement on future rainfall change is very limited, with changes over northern and central Australia showing large uncertainties and even incongruities regarding the sign of change (Irving et al., 2012), particularly in summer and autumn (Moise et al., 2015). For example, Irving et al. (2012) show that projected changes of March-April-May mean precipitation over north-west Australia have a multi-model ensemble mean of +0.4, but an inter-model standard deviation of ±24.5%. The models also show large uncertainties in projections of the Australian summer monsoon, with models ranging from a 40% increase to a 40% decrease in monsoonal rainfall due to model biases in SSTs (Brown et al., 2016). Overall, Brown et al. (2016) found that precipitation change in the Australian monsoon among models was strongly negatively correlated with SST changes in the western tropical Pacific. Meanwhile, CMIP5 models seem to be able to project temperature changes over Australia with more clarity, with projected changes by 2090 being 4.2 ±0.9°C for RCP8.5 (Irving et al., 2012). This dissertation will assess how differences between models in future projections of the Bilybara High may help to explain intermodel differences in rainfall and temperature projections.

Section 2: Data & Methods

First, this section will outline the details of the ERA5 reanalysis data and data from a selection of models within the CMIP5 database used to study the Bilybara High and its impacts on rainfall and temperature. All data used in this study has been acquired from the Oxford University School of Geography and the Environment data catalogue. Secondly, this section will outline the methodology undertaken to produce the plots seen in this study.

This study will be looking at variables of rainfall and temperature averages, as well as dry day, heavy rainfall, and high temperature frequency. These factors can be used as good parameters for drought, and therefore researching them both in the present data and in future predictions is of importance to a number of stakeholders.

2.1 Data

ERA5 Reanalysis Data

Reanalyses are commonly used datasets in climate science as they provide a high quality and comprehensive description of the observed climate on three-dimensional grids with temporal resolutions as high as hourly. The reanalysis dataset used is in this study is ERA5. ERA5 is the most recent climate reanalysis dataset produced by the European Centre for Medium-Range Weather Forecasts (ECMWF) (Hersbach et al., 2020). The dataset combines historical observations into global estimates using advanced modelling and data assimilation systems (ECMWF, 2020). ERA5 provides atmospheric, land, and oceanic climate parameters, with a resolution of 0.25°x0.25° and 137 atmospheric pressure levels, and also contains estimates of uncertainty for all variables (ECMWF, 2020).

This study uses daily data from ERA5 for the month of March. March is chosen because it is when the maximum strength of the Bilybara High occurs on an annual cycle (Figure 4). For general plots (Figures 3 and 4) in Section 1, the time period 2000-2018 is used because it is the most recent period that includes all variables. For plots seen in Section 3 (Figures 7-15), the time period 1980-2005 is used. This was chosen to coincide with the time period used for the historical model simulations to enable direct comparisons. The two time periods chosen were also selected because all variables had complete datasets for these periods.

The variables used from the ERA5 dataset are geopotential height (GPH), 2-metre temperature, total precipitation, the Universal Thermal Climate Index (UTCI), and vertical velocity. The UTCI is a

human thermal stress indicator (Kampmann et al., 2013) that has recently been released by ECMWF and is used briefly in this study to show the intersection between climate (specifically the Bilybara High) and human health.

Climate Models

Daily data in March from a selection of 20 CMIP5 models are used in this study, with model details shown in Table 1. These were selected based upon the availability of the necessary variables. All models contain GPH, near-surface temperature, and precipitation data for both historical and RCP8.5 outputs. The only exception is FGOALS-g2 which has no RCP8.5 output for temperature. All models have been remapped to a common grid size of 2°x2° so that the spatial resolutions are constant.

This study will compare the end of the 20th century to the end of the 21st century, with two 25-year periods being chosen: 1980-2005 for historical simulations and 2075-2100 for RCP8.5 simulations. Historical simulations are forced with predetermined solar irradiance, gaseous chemical and aerosol concentrations, basic land use, and changing atmospheric compositions due to anthropogenic influence (IPCC, 2013). RCP8.5 simulations are forced with a pathway that results in a radiative forcing of 8.5 W m^{-2} at 2100 relative to pre-industrial conditions (IPCC, 2013).

Model Name	Institution and Location
ACCESS1-0	Commonwealth Scientific and Industrial Research, Organization and Bureau of Meteorology, Australia
ACCESS1-3	Commonwealth Scientific and Industrial Research, Organization and Bureau of Meteorology, Australia
BCC-CSM1-1-m	Beijing Climate Centre, China Meteorological Administration, Beijing, China
BNU-ESM	College of Global Change and Earth System Science, Beijing Normal University, Beijing, China
CanESM2	Canadian Centre for Climate Modelling and Analysis, Victoria, BC, Canada
CMCC-CESM	Centro Euro- Mediterraneo per I Cambiamenti Climatici, Lecce, Italy
CMCC-CM	Centro Euro- Mediterraneo per I Cambiamenti Climatici, Lecce, Italy
CMCC-CMS	Centro Euro- Mediterraneo per I Cambiamenti Climatici, Lecce, Italy
FGOALS-g2	Institute of Atmospheric Physics, Chinese Academy of Sciences, Beijing, China
GFDL-CM3	Geophysical Fluid Dynamics Laboratory, National Oceanic and Atmospheric Administration, Princeton, NJ, USA
GFDL-ESM2G	Geophysical Fluid Dynamics Laboratory, National Oceanic and Atmospheric Administration, Princeton, NJ, USA
HadGEM2-CC	Met Office Hadley Centre, Exeter, UK
HadGEM2-ES	Met Office Hadley Centre, Exeter, UK
IPSL-CM5A-MR	L'Institut Pierre-Simon Laplace, Paris, France
MIROC5	Japan Agency for Marine-Earth Science and Technology, Atmosphere and Ocean Research Institute (The University of Tokyo), and National Institute for Environmental Studies, Tsukuba, Japan
MIROC-ESM	Japan Agency for Marine-Earth Science and Technology, Atmosphere and Ocean Research Institute (The University of Tokyo), and National Institute for Environmental Studies, Tsukuba, Japan
MIROC-ESM-CHEM	Japan Agency for Marine-Earth Science and Technology, Atmosphere and Ocean Research Institute (The University of Tokyo), and National Institute for Environmental Studies, Tsukuba, Japan
MPI-ESM-MR	Max Planck Institute for Meteorology, Hamburg, Germany
MRI-CGCM3	Meteorological Research Institute, Tsukuba, Japan
NorESM1-M	Norwegian Climate Centre, Bergen/Oslo, Norway

Table 1 – List of CMIP5 models used in this study.

2.2 Methods

Here the methods used for each plot are detailed. The regions used in the study are displayed in Figure 5. These regions were chosen based upon the relevant composite anomalies. Climate Data Operators and Python code have been used to manipulate datasets and produce plots. Copies of example scripts used in the production of the plots can be found in Appendix B.

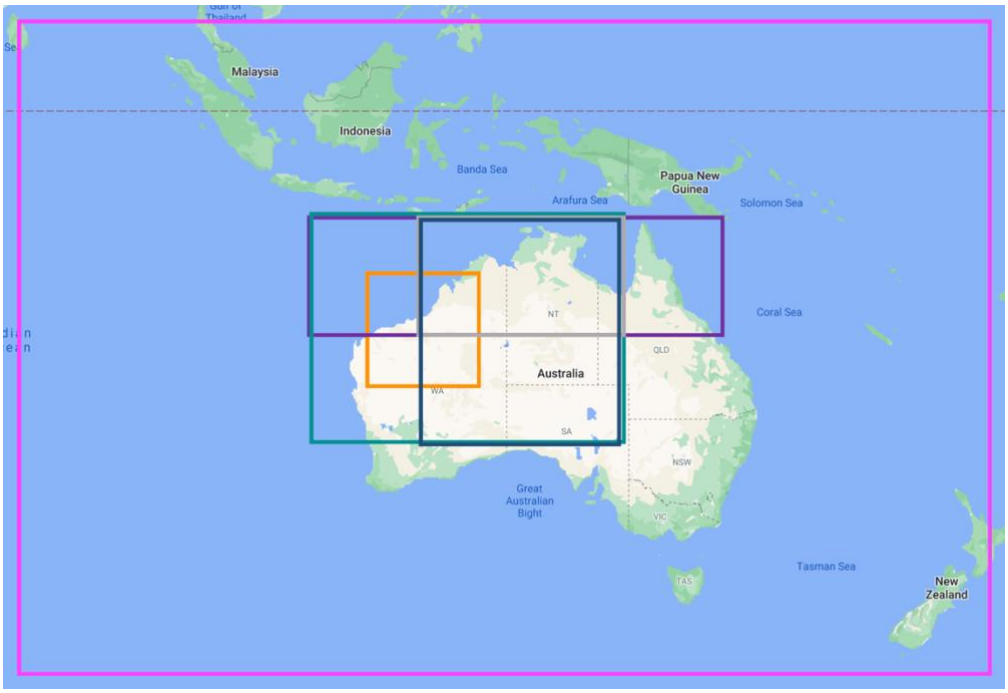

Figure 5 – Regions used for methods. Larger Australia area, 80-175°E 10°N-50°S (pink box). Core region of the Bilybara High, 115-125°E 15-25°S (orange box). Precipitation for the scatter plots, 110°-150°E 10°-20°S (purple box). Temperature for the scatter plots, 110°-140°E 10°-30°S (green box). Heavy precipitation and dry day frequency for the scatter plots, 120°-140°E 10°-20°S (grey box). High temperature frequency for the scatter plots, 120°-140°E 10°-30°S (dark blue).

Bilybara High Indices

Two indices, a standardised anomaly and a relative anomaly, are created to identify the strength of the Bilybara High on individual days. These indices are calculated for ERA5 data and each model. The standardised anomaly index is used for all map plots and was produced by spatially averaging the 500hPa GPH over the core region of the High and plotting the standardised anomalies. A standardised anomaly index is used because they generally provide more information about the size of the anomalies as the influences of data dispersion have been removed. Similar methods have also been seen in other papers, for example, Driver and Reason (2017) and Reason (2018). The relative anomaly index is used for the scatter plots (Figures 31 and 32) and was produced by subtracting the spatially averaged larger Australia area 500hPa GPH from the spatially averaged 500hPa GPH over

the core region of the High (see domains in Figure 5). A relative anomaly index is used because a physically based index that is relative to the GPH at the time is needed so that direct comparisons can be made between historical and RCP8.5 model simulations. The standardised anomaly index is not used to assess future change because as temperature increases so do GPH values as the air column deepens with warming, and so the results would conflate thermodynamic with dynamic changes.

The standardised anomaly Index (Figure 6) shows the strength of the High from 1980-2005 on a daily basis in March. The Index is used to select 'no', 'weak' or 'strong' High day percentiles that can be used in upcoming plots. As can be seen in Figure 6, the strength of the High ranges from standardised anomalies of 5.5 to -9.5 and it is evident that the strength of the High can vary quite significantly from day to day and from year to year.

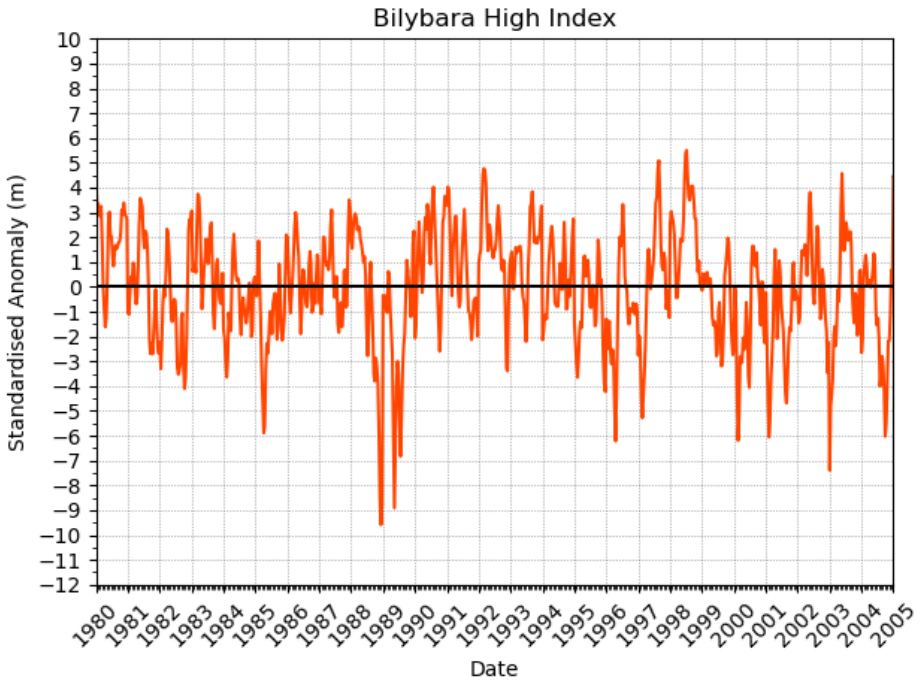

Figure 6 – An index for the Bilybara High obtained from the standardised anomaly in 500hPa GPH (m) for March averaged over 115-125°E, 15-25°S.

Threshold Definitions

Thresholds have been defined for no, weak and strong Bilybara High conditions. These were defined by testing a range of thresholds on GPH composite plots. No High was present in plots below the 20th percentile of the High Index; these are termed 'no High days'. No High days are compared with 'strong High days' – above the 80th percentile of the Index. Meanwhile, 'weak High days' use the 60th-80th percentiles of the Index. These thresholds are used for all plots to select data to show no,

weak or strong High days. This enables comparisons to be made regarding the effects of the strength of the High on different climatic variables. An anomaly is also produced for each variable to show the difference between the strong and no High days. For figures in Section 3 that contain multiple plots there are 4 maps: no, weak and strong High days, and an anomaly of strong-minus-no High days. In Sections 4 and 5 only the anomaly plots are used for a more succinct and clear display of the impact of the Bilybara High.

Correlations

In Section 3 Pearson's Correlation Coefficients (Equation 1) are calculated between the Bilybara High Index and precipitation and temperature. Correlation coefficients and associated p-values are calculated, and the regions on the map that show a statistically significant (based on t-tests) correlation are indicated by stipples. Pearson's is also used to calculate the correlation between variables in the scatter plots (Figures 31 and 32).

$$\boldsymbol{r = \frac{\sum(x_i - \bar{x})(y_i - \bar{y})}{(n-1)s_x s_y}}$$

Equation 1 - Where r = Pearson's Correlation Coefficient, n = number of data points, (x_i, y_i) = individual (x, y) values, ($\bar{x}$, $\bar{y}$) = mean of all (x_i, y_i), (s_x, s_y) = the standard deviation of (x, y).

Composites

Composites are produced for each variable. Composites are the average of a variable taken over a specific time period (in this case 1980-2005 or 2075-2100) and have been computed using daily averages in March. Composites are useful when looking at a specific climate feature because they pool the signal and cancel out noise from internal variability so repeated features, such as the Bilybara High, show up.

Extreme frequencies

Extreme frequency plots are produced to study the impacts of the Bilybara High on extreme rainfall and temperature. For the ERA5 dataset four sets of plots have been produced: extreme dry day frequency, extreme heavy rainfall frequency, extreme high temperature frequency and extreme high UTCI frequency. For the historical and RCP8.5 model simulations, three sets of plots have been produced: extreme dry day frequency, extreme heavy rainfall frequency and extreme high temperature frequency. The plots were produced by calculating the relative number of days within

the dataset that exceeded the 90th percentile of the variable dataset (except for dry day frequency which selected days that were below the 10th percentile).

Section 3: The Bilybara High

This section builds on the existing literature (Reason, 2016; Reason, 2018) to clarify the relationships between the Bilybara High and mean rainfall and temperature in high-resolution ERA5 data for March at daily timescales. Section 3.3 then considers the relationship between the High and extreme rainfall and temperature for the first time.

3.1 Identifying the Bilybara High

Firstly, the Bilybara High is identified using ERA5. Figure 7 shows composite plots of GPH for strong, weak and no High days. On days when there is no High evident, GPH sits at around 5780m. For weak High days, a high-pressure system is evident, but this has a maximum GPH of 5840m and only covers a small region. On strong High days, the High is much clearer, with a large high-pressure system of GPH 5870m covering much of western Australia and a small section of the Indian Ocean. Looking at the anomaly plot, the core region of the Bilybara High is concentrated over north-west Australia, with the GPH anomaly lessening but remaining positive as we move away from the High. The anomaly plot is clear evidence of the difference in GPH between the days when there is no High and when the High is strong, with a difference in GPH of approximately 90m.

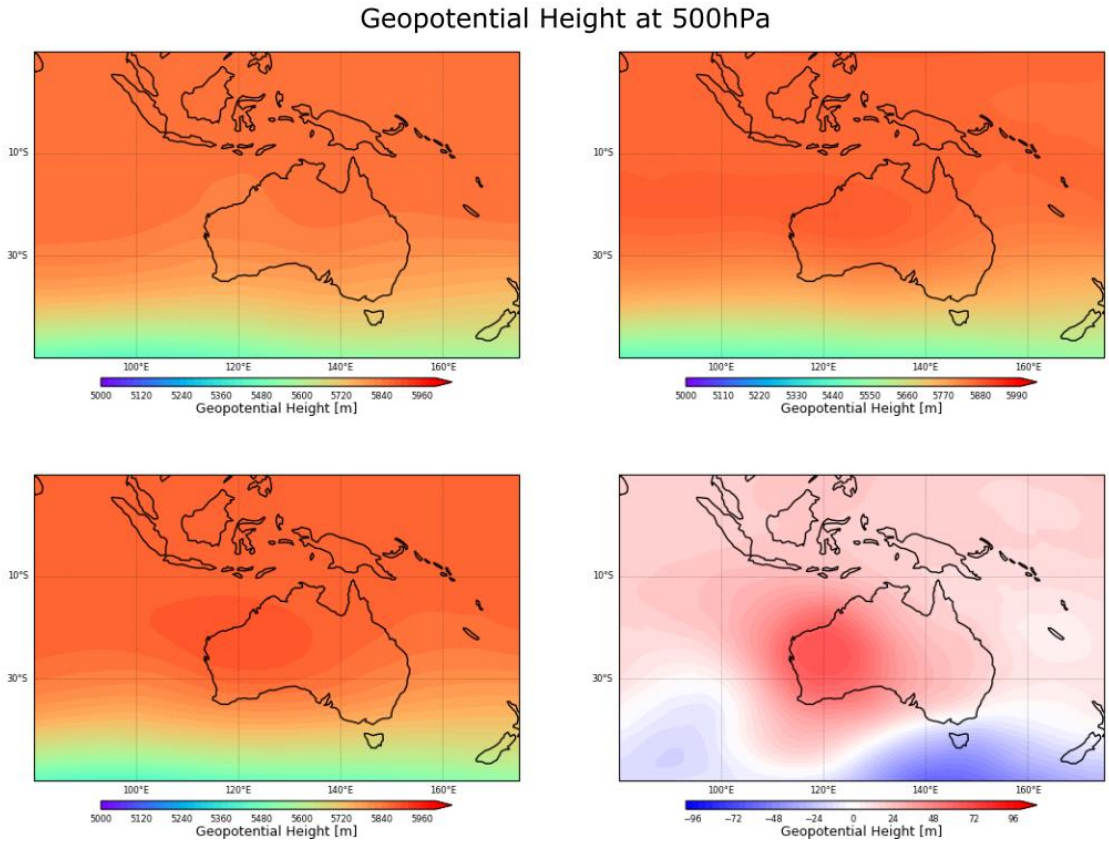

Figure 7 – GPH (m) composites are used to identify the High and its magnitude over Australia for March. The plots are composites of no (top left), weak (top right) and strong (bottom left) High days, and an anomaly of strong-minus-no High days (bottom right).

3.2 The Bilybara High and mean climatology

3.2.1 Rainfall

First, the relationship between the Bilybara High Index and rainfall is interrogated. Figure 8 shows their spatial correlation. There is a statistically significant moderate to strong negative correlation (r = -0.3 to r = -0.5) over a large part of Australia and part of the Ocean to its north, meaning that as the strength of the High increases, mean rainfall decreases. This result shows that the relationship between interannual variability in the High and rainfall identified by Reason (2018) also holds at daily timescales. Interestingly, however, there seems to be a weak positive correlation (r = 0.2) between the Index and rainfall over parts of the Maritime continent, namely the Indonesian landmasses.

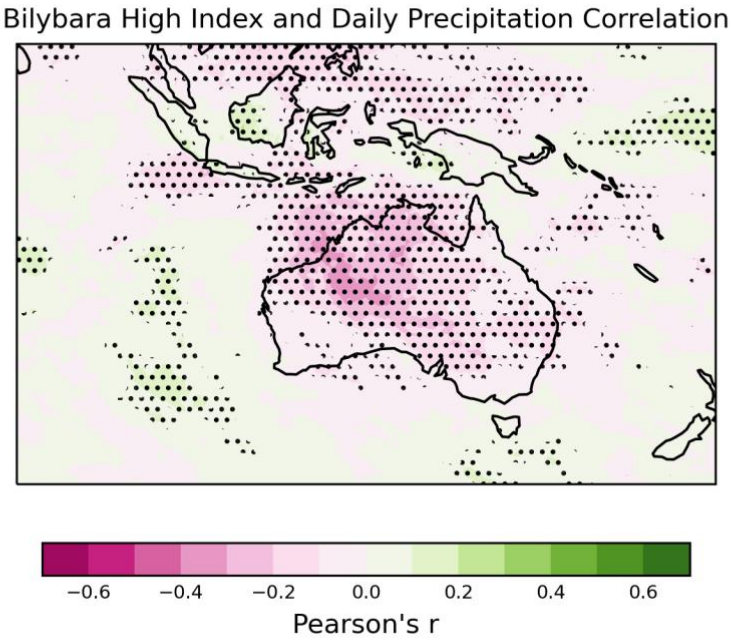

Figure 8 – Pearson's Correlation Coefficient values showing the spatial correlation of the High Index and daily rainfall across Australia for March.

The relationship between the strength of the High and rainfall can further be seen in the composite plots (Figure 9). The anomaly plot clearly shows how rainfall varies depending on the strength of the High. Ultimately, when the High is strong there is much less rainfall occurring across northern Australia, with the largest anomaly value being -16 mm/day of rainfall over the north-west. Rainfall over the north-west of Australia seems to be the most impacted by the strength of the Bilybara High. Meanwhile, southern Australian rainfall seems to have little relationship with the High, which makes sense given the climatological location of the High. The main pattern is that on days when the High

is strong average rainfall is close to 0mm, which is a significantly reduced level from days when there is no High. This is because the High sits over the region of north-western Australia and suppresses rainfall by creating clear skies. Interestingly, as is seen in both the correlation and composite plots, a strong High is associated with increased local rainfall over parts of the Maritime continent landmass, despite the positive GPH anomaly values over this region seen in Figure 7. There are a few possible reasons for this. Potentially, the enhanced diabatic heating associated with convection over the Maritime continent increases the strength of the High. Alternatively, in some way the presence of the High results in this increase in rainfall further north. This is not consistent with Figure 3, which shows reduced uplift over the Maritime continent on days when the High is stronger. Although this study will not further examine the reasoning behind this, it is an interesting pattern to note.

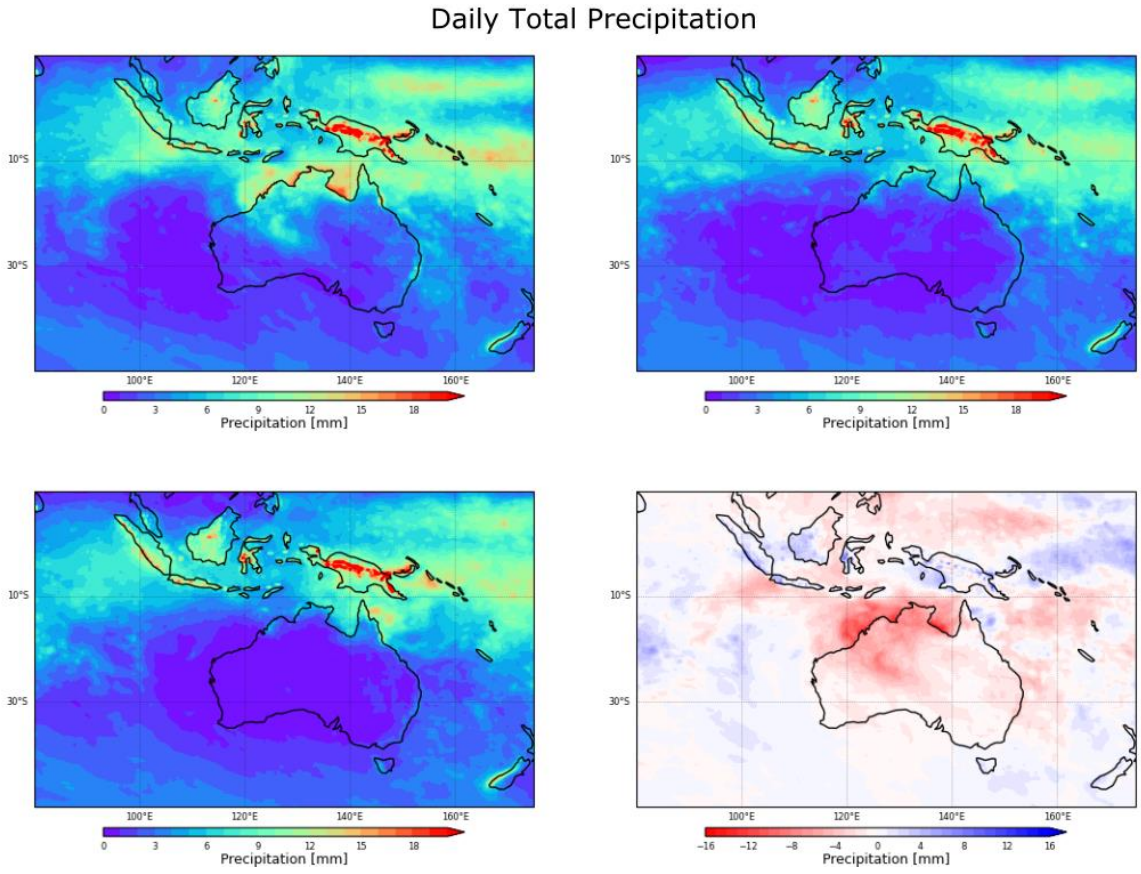

Figure 9 – Composites of daily total rainfall (mm day^{-1}) showing how levels are influenced by the strength of the High in March. The plots are composites of no (top left), weak (top right) and strong (bottom left) High days, and an anomaly of strong-minus-no High days (bottom right).

These plots of mean rainfall show similar patterns to those shown by Reason (2016, 2018) whereby a stronger (weaker) midlevel anticyclone is associated with anomalously dry (wet) conditions.

3.2.2 Temperature

To investigate the relationship with temperature, Figure 10 shows the spatial correlation between the Bilybara High Index and mean near-surface temperature in March. There is a very clear statistically significant strong correlation with temperature that covers the majority of the Australian landmass as well as a significant proportion of the surrounding oceans. Over the core region of the High, this correlation reaches a Pearson's coefficient of 0.6 which highlights the significant influence the High can have on temperature.

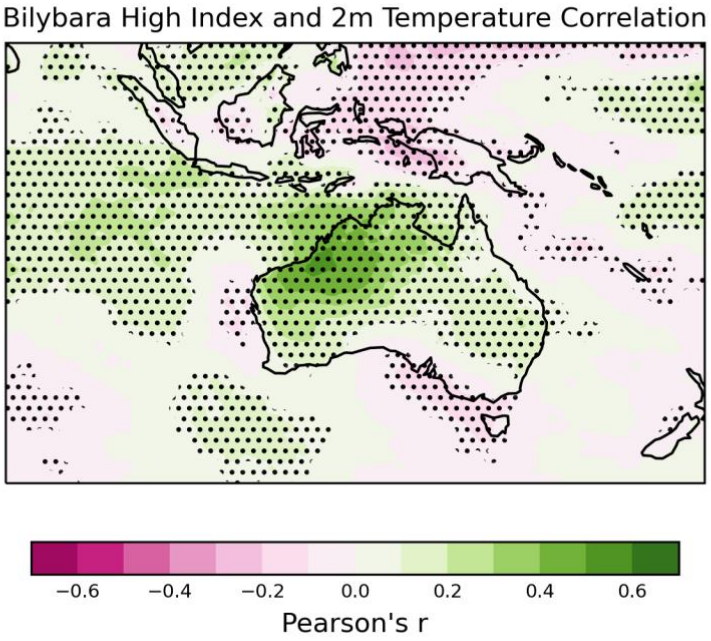

Figure 10 - Pearson's Correlation Coefficient values showing the spatial correlation of the High Index and daily near-surface temperature across Australia for March.

The positive relationship between the High and temperature shown in Figure 10 is further investigated using the composite means of near-surface temperature. These composites are seen in Figure 11 and show that there are significant temperature increases over the majority of western Australia during strong High days compared to no High days, with temperatures rising by up to 7°C at the core High region. This relationship between the High and near-surface temperature is expected as a stronger high-pressure system results in clearer skies which in turn allows for increased incoming solar radiation, so the net radiation balance is likely to be anomalously positive. There is also a small area on the southern Australian coast, which shows an opposite pattern to the rest of the landmass. The Figure shows that over this region there are lower temperatures when the High is stronger. The reasoning for this is unknown and could be of interest to examine in future research.

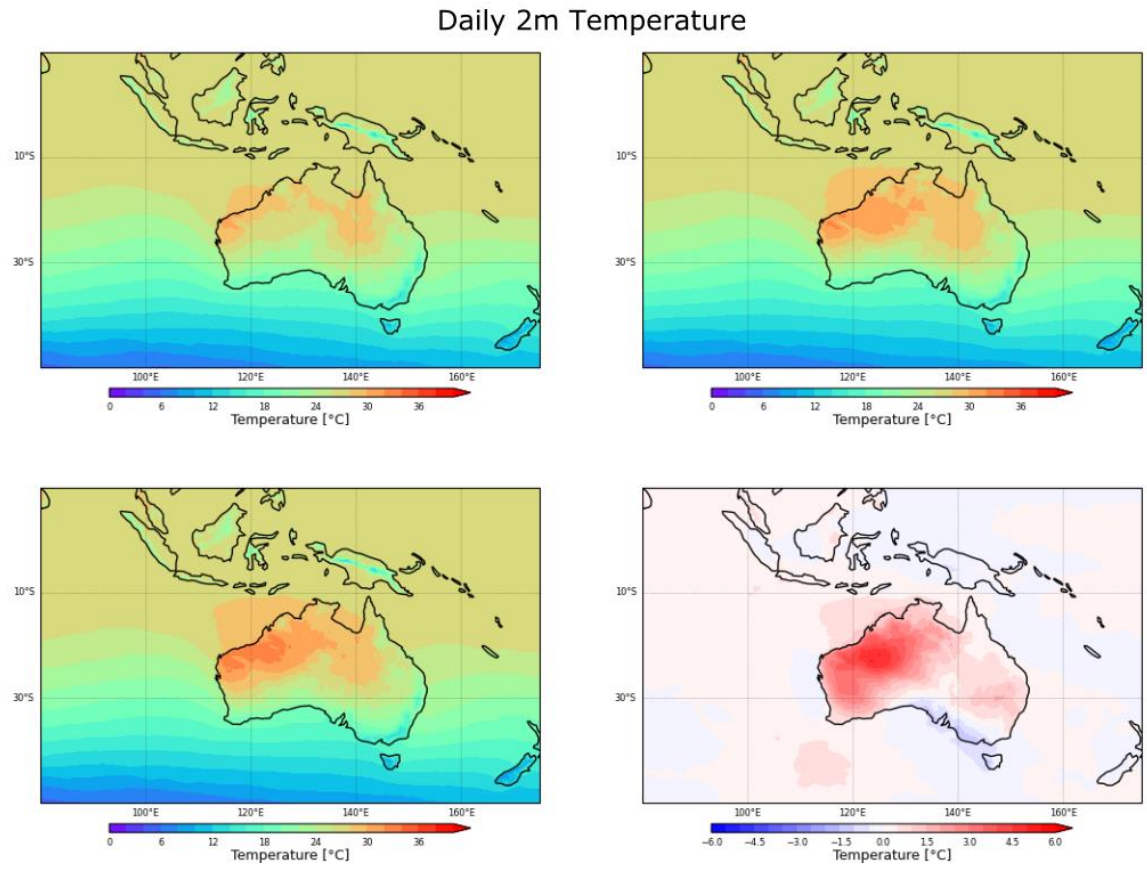

Figure 11 – Composites of daily near-surface temperature (°C) showing how they are influenced by the strength of the High in March. The plots are composites of no (top left), weak (top right) and strong (bottom left) High days, and an anomaly of strong-minus-no High days (bottom right).

Reason (2018) showed that the Bilybara High influences maximum surface air temperature over Australia whereby a stronger High is associated with higher temperatures across large areas of the landmass. These plots clarify the relationship between the High and temperature by looking at daily mean temperatures and finding similar results.

3.3 The Bilybara High and extreme climatology

As well as mean rainfall and temperature, the strength of the Bilybara High may affect the frequency of extreme climatology. It is important to investigate the effects on extreme climatology because they often result in extreme weather events such as drought. Hence, this sub-section presents the relative frequency of days with low rainfall, heavy rainfall, and high temperature. We also briefly discuss the extreme levels of the UTCI to explore the intersection between the Bilybara High and human health.

3.3.1 Rainfall

The relative frequency of extreme dry days (days below the 10th percentile of the dataset) is displayed in Figure 12. This extreme shows an interesting pattern of how the Bilybara High impacts extreme low rainfall days over Australia. In the north of Australia, there is a higher relative frequency of dry days with a stronger High, reaching a 38% increase between no and strong High days. This result is expected because in the previous sub-section we saw that the high-pressure system suppresses rainfall. However, looking at the south of Australia a decrease in the relative frequency of dry days is present for a stronger High. This is unusual as previous rainfall plots show that the High has a limited relationship with southern Australia.

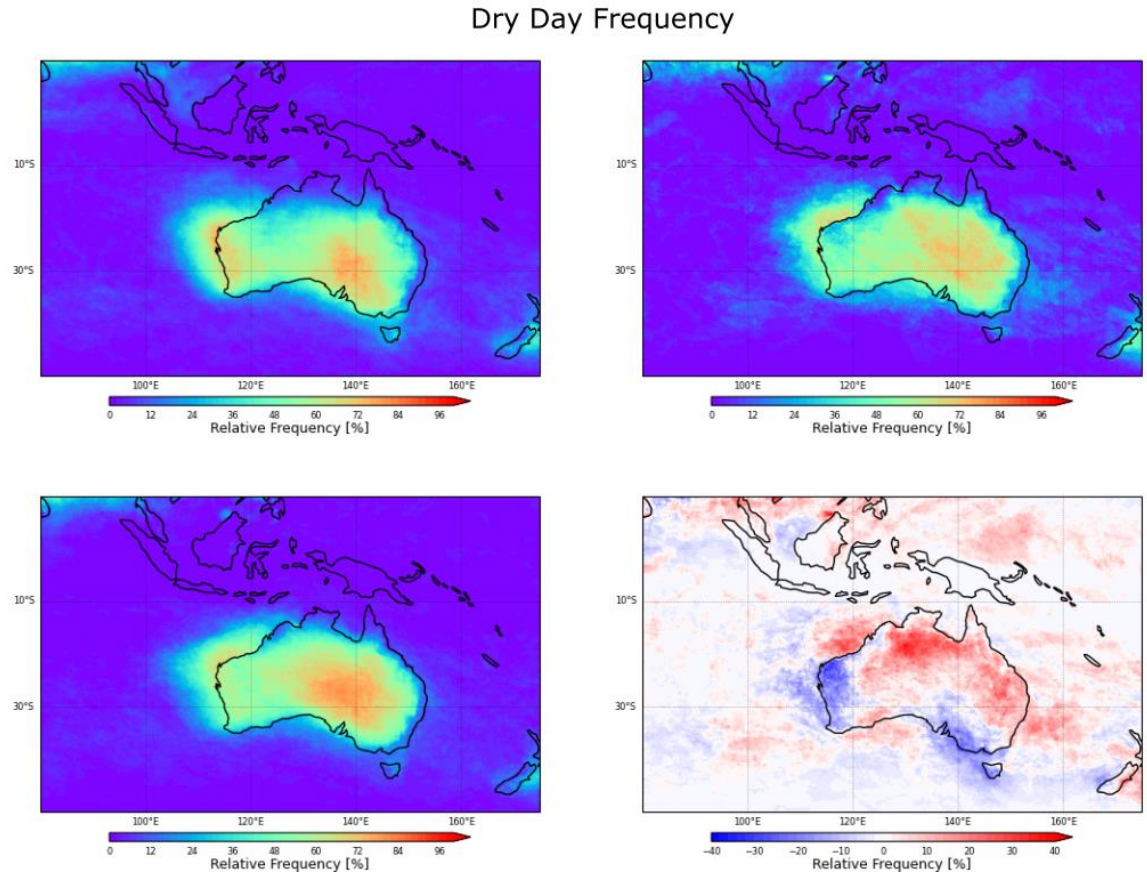

Figure 12 – Composites showing the relative frequency of extreme dry days at differing High strengths in March. The plots are composites of no (top left), weak (top right) and strong (bottom left) High days, and an anomaly of strong-minus-no High days (bottom right).

The Bilybara High also has an impact on extreme heavy rainfall. This is shown in Figure 13. The relative frequency of extreme heavy rainfall days (days above the 90th percentile of the dataset) shows that a strong High results in a decreased frequency of extreme heavy rainfall days (of up to 34%), compared to no High, that is concentrated over a large part of north-western Australia. Interestingly, consistent with the mean rainfall plots (Figure 9), a strong High is associated with increased frequency

of extreme rainfall over the Maritime continent (maximum relative frequency increase of 25%). In fact, the relationship is much clearer when looking at heavy rainfall frequency compared to mean rainfall. Examining the physical processes linked to heavy rainfall over the Maritime continent and the Bilybara High should be of interest for future research.

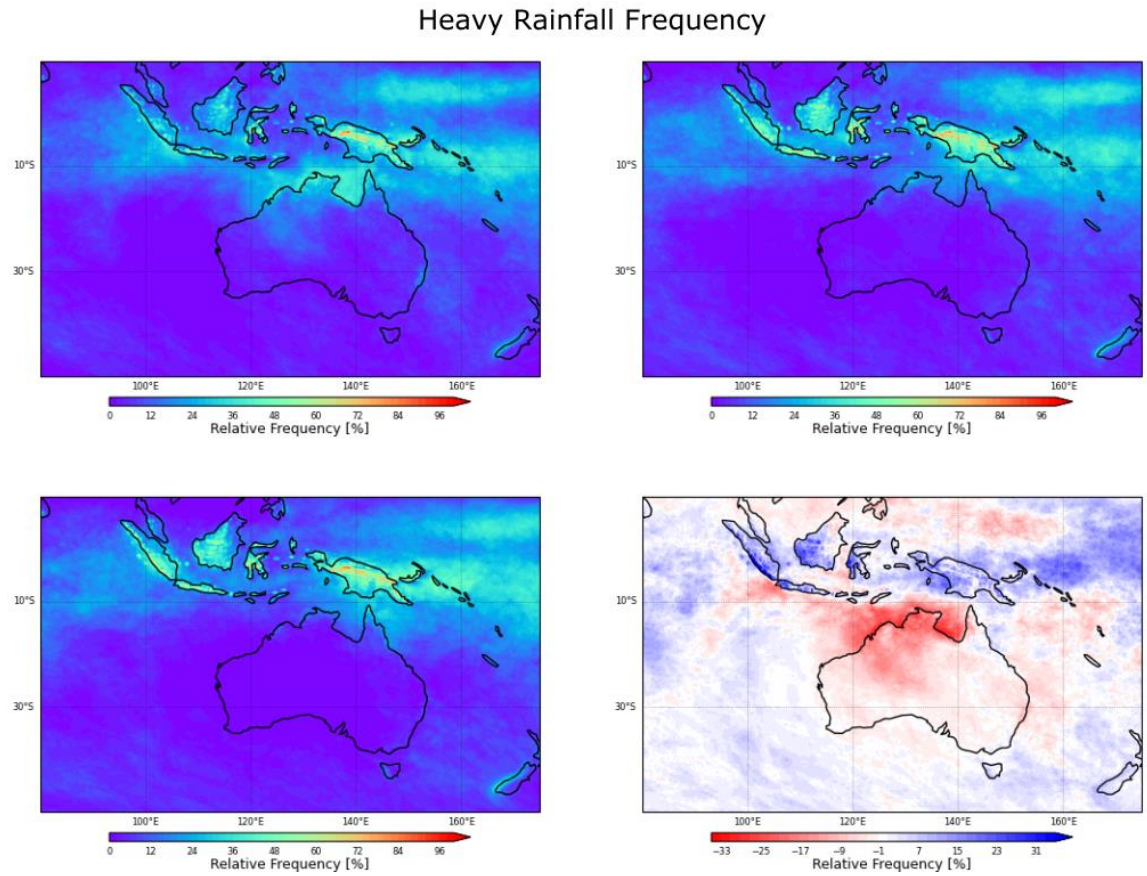

Figure 13 – Composites showing the relative frequency of extreme heavy rainfall days at differing High strengths in March. The plots are composites of no (top left), weak (top right) and strong (bottom left) High days, and an anomaly of strong-minus-no High days (bottom right).

3.3.2 Temperature

To investigate the relationship with extreme temperature, Figure 14 shows the relative frequency of extreme high temperature days. The plots show that the High has a large spatial impact on the relative frequency of extreme high temperature days, with the majority of western and central Australia showing large increases (up to 37%) from no to strong High days. Interestingly, the Figure shows a decrease in the relative frequency of extreme temperature days over the Maritime continent. Interestingly, this cannot be clearly seen in the mean temperature plots.

Reason (2018) briefly addresses the relationship between the Bilybara High and the number of days exceeding the 90th percentile in surface air temperature for January to March, concluding that the

drier conditions associated with a stronger High are compounded by increases in the number of days with extreme temperatures over large areas of Australia. The findings in this study based on daily ERA5 data match up to those found by Reason (2018), providing strong evidence that the High has a significant impact on temperature characteristics over Australia.

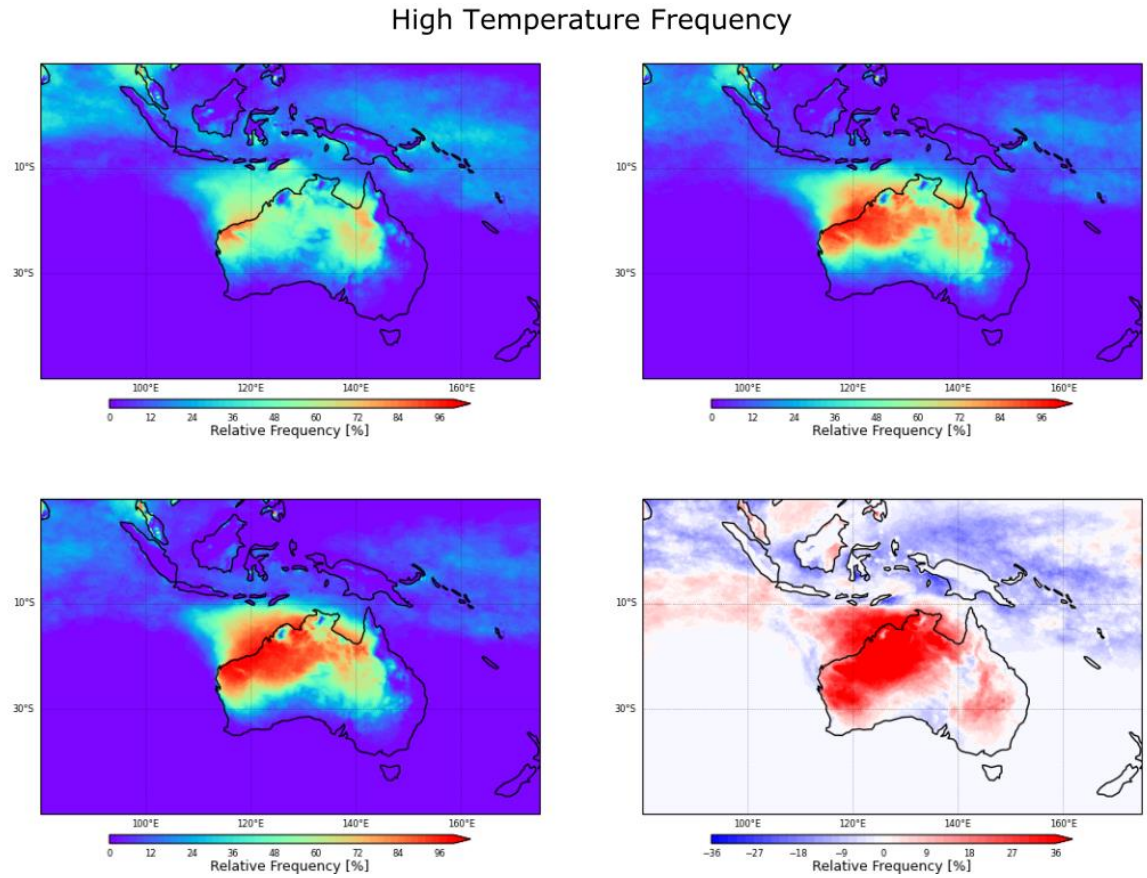

Figure 14 - Composites showing the relative frequency of extreme high temperature days at differing High strengths in March. The plots are composites of no (top left), weak (top right) and strong (bottom left) High days, and an anomaly of strong-minus-no High days (bottom right).

Extreme hot and dry conditions (as seen in Figures 14 and 12, respectively) can also have significant impacts on human health, with heat stress causing severe discomfort and illness, especially for vulnerable groups such as the elderly and infants (Gallant et al., 2018; Arriagada et al., 2019). Heat stress can affect the psychological (Tawatsupa et al., 2012) and physiological (Tian et al., 2011) wellbeing of people. Monitoring heat stress experienced by people can be a clear indicator of the social impacts of temperature extremes. Therefore, this sub-section will concisely discuss the impact of the Bilybara High on the UTCI.

Figure 15 shows the relative frequency of extreme high UTCI days. Very similar patterns are seen as with extreme near-surface temperature frequencies, with increases of up to 41% from no to strong High days. This is unsurprising as the UTCI is based upon temperature related variables. Nonetheless,

it is interesting to note the direct link between the Bilybara High and human health, with that link being extremely strong. It is important to note that the UTCI seems to have a slightly reduced spatial extent to near-surface temperature, with the influence of the High being seen only over north-western Australia and closer to the coast. This spatial pattern coincides with the fact that closer to the coast is likely to be more humid, and humidity is included in the calculation of the UTCI.

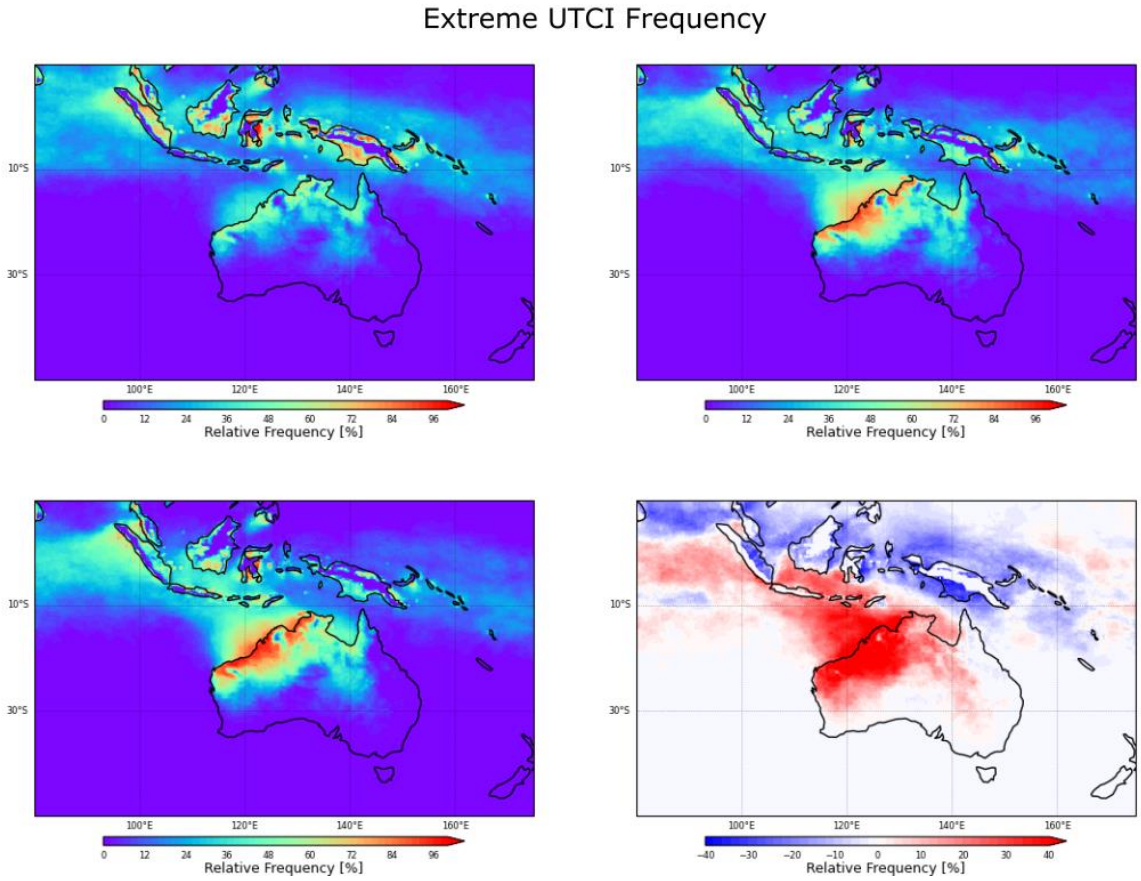

Figure 15 - Composites showing the relative frequency of extreme high UTCI days at differing High strengths in March. The plots are composites of no (top left), weak (top right) and strong (bottom left) High days, and an anomaly of strong-minus-no High days (bottom right).

3.4 Overview of the Bilybara High and its impacts on rainfall and temperature in high-resolution ERA5 reanalysis data

Section 3 has provided evidence, using ERA5, that there are robust relationships between the strength of the Bilybara High and rainfall and temperature, for both mean and extreme climatologies. Reason (2018) had previously shown that the Bilybara High influenced mean rainfall and temperature, and this has been further proven with high-resolution reanalysis data at daily timescales. We have also shown that the High has a significant influence on extreme climatologies. What is interesting to note is the spatial extent of the influence. The Bilybara High seemingly has an impact on temperature on

a large spatial scale, expanding further than rainfall, which could become very important in the future regarding the potential negative consequences of increasing and extreme temperatures.

The next section considers how these relationships are shown in the CMIP5 models. The leading question is whether climate models are able to reproduce these relationships. First, we must evaluate how well the models reproduce the Bilybara High, and then we go onto look at the relationship between the High and rainfall and temperature means and extremes.

Section 4: Historical representation of the Bilybara High in CMIP5

This section considers the simulations of the High in climate models for March. First, we look at the historical simulation as compared to ERA5. Then we assess whether the present-day simulations are able to produce the clear relationships with temperature and rainfall that are shown in the previous section.

4.1 Historical simulation of the High in CMIP5 models

In general, the CMIP5 models perform well in representing the Bilybara High in March. This is evident in Figure 16, which shows the anomaly of strong-minus-no High days in 20 models. Almost all models display a high-pressure system at 500hPa over the core region of the High, with this high-pressure system reducing in intensity from the core but expanding over a large part of western Australia. The only exception is the CMCC-CESM model which shows no significant difference between strong and no High days over Australia, and a very weak high-pressure system off the north-west coast over part of the Indian Ocean. The main difference between model portrayals of the High is the maximum anomaly of the strength of the High. For example, the model with the strongest anomaly at the High centre is CMCC-CMS with a maximum GPH anomaly of 98m, while the weakest GPH anomaly of 48m is seen in model MRI-CGCM3.

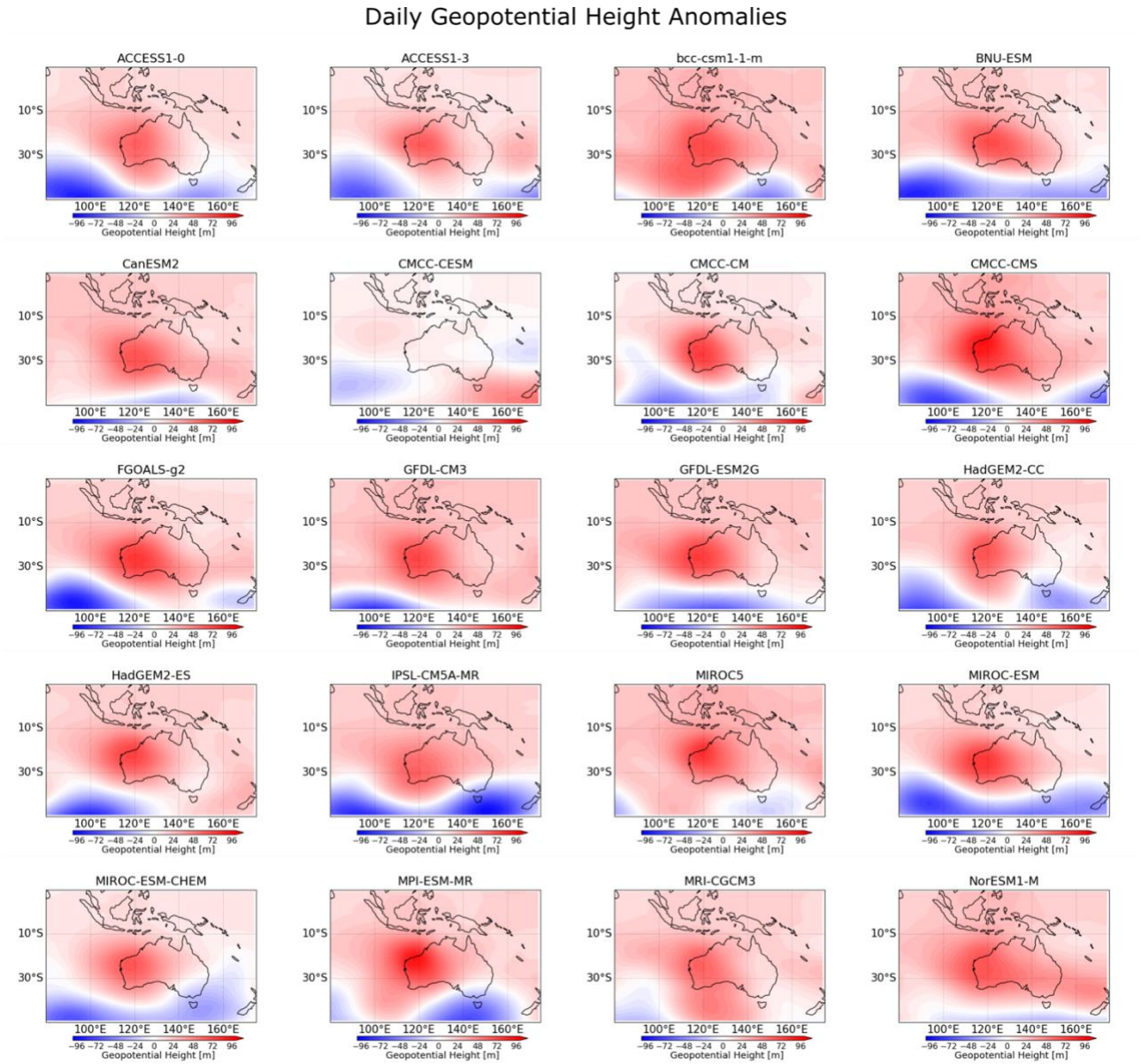

Figure 16 – Anomaly composites (strong-minus-no High days) of daily geopotential height (m) at 500hPa for 20 CMIP5 historical simulations for March.

It is important to know whether the historical simulations used in this study underestimate or overestimate the strength of the Bilybara High. Overestimates are likely to result in more exaggerated impacts on rainfall and temperature whereas underestimates are likely to mean reduced impacts. Figure 17 shows the threshold for strong High days for each model and ERA5. This indicates the GPH value for the 80th percentile of the Index, and so essentially shows the maximum strength of the High as the higher the GPH the stronger the high-pressure system at 500hPa. Overall, thirteen models underestimate the strength of the High, and seven overestimate it compared to ERA5. MIROC-ESM severely overestimates the strength of the High by almost 125m. Other significant overestimates include BCC-CSM1-1m and CMCC-CESM, but these are to lesser extents. Meanwhile, GFDL-ESM2G considerably underestimates the strength of the High, with the GPH being almost 50m less.

With the exception of MIROC-ESM, there are relatively small intermodel differences in the strength of the High, and they all perform reasonably well with respect to ERA5.

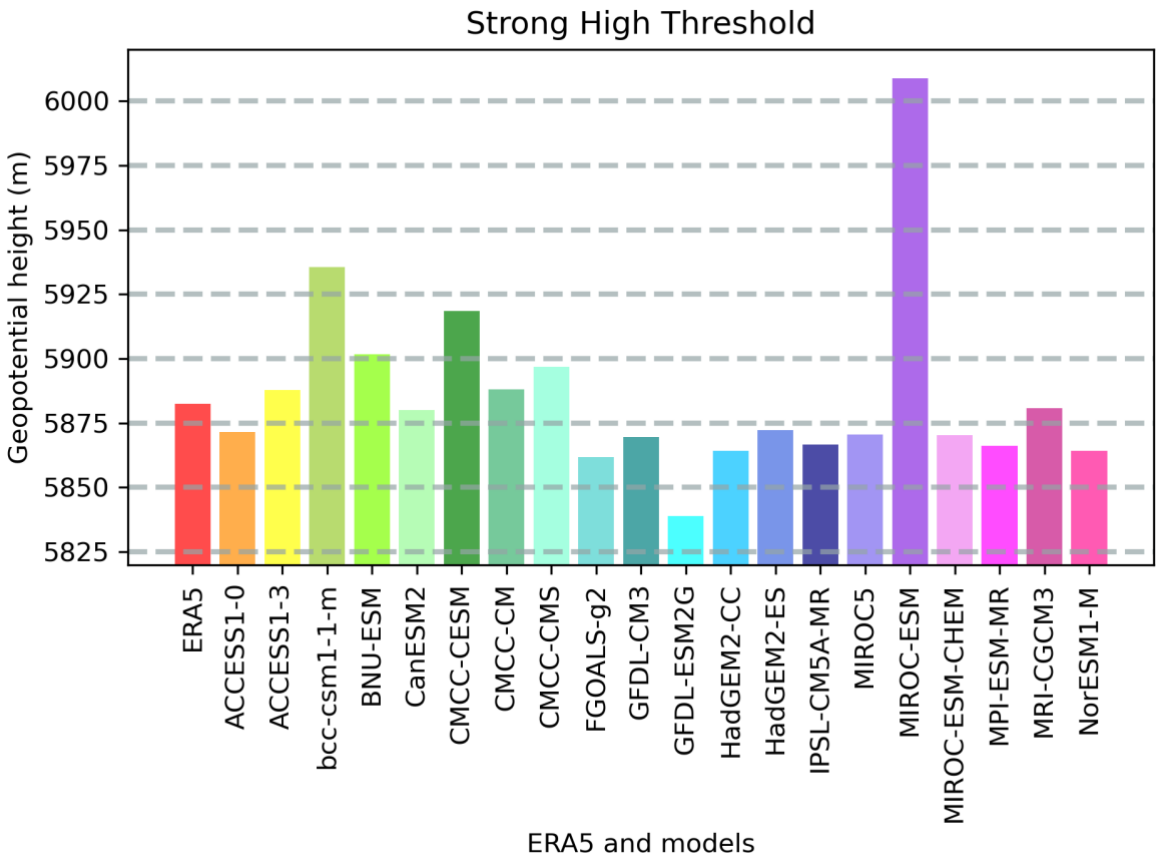

Figure 17 – A bar graph showing the strong High threshold (the 80th percentile of the standardised anomaly High Index) for each model compared to the ERA5 threshold (first red bar) for March.

Overall, while all models capture the Bilybara High, there are some intermodel differences. The following sub-section aims to investigate whether models are able to reproduce the relationship between the High and rainfall and temperature, as in ERA5.

4.2 How well do the models produce the relationships between the High and rainfall and temperature?

4.2.1. Rainfall

In this section, we consider the relationship between the High and rainfall. Analogous to ERA5, models generally simulate lower rainfall in northern and central Australia on days with a strong high, while there is an increase in rainfall over the Maritime continent. This is shown in Figure 18. No models show exactly the same relationship between the strength of the High and rainfall, but the

majority are able to represent the overall pattern. Dissimilarities become apparent in maximum rainfall changes and the spatial extents of these changes. CanESM2, CMCC-CESM and IPSL-CM5A-MR do not accurately represent the relationship between the High and rainfall that is shown in the ERA5 data (Section 3). These models have very little to no rainfall change over Australia between strong and no High days. For CMCC-CESM, this can most likely be explained by the model's poor representation of mid-level GPH (Figure 16). It is less clear why CanESM2 and IPSL-CM5A-MR fail to produce the correct relationship. Furthermore, while the majority of models show the increase in rainfall over the Maritime continent, CMCC-CM and CMC-CMS instead show a decrease or no change in rainfall over this area during stronger High days. This puts into question their ability to comprehensively represent the spatial extent of the relationship between the High and rainfall.

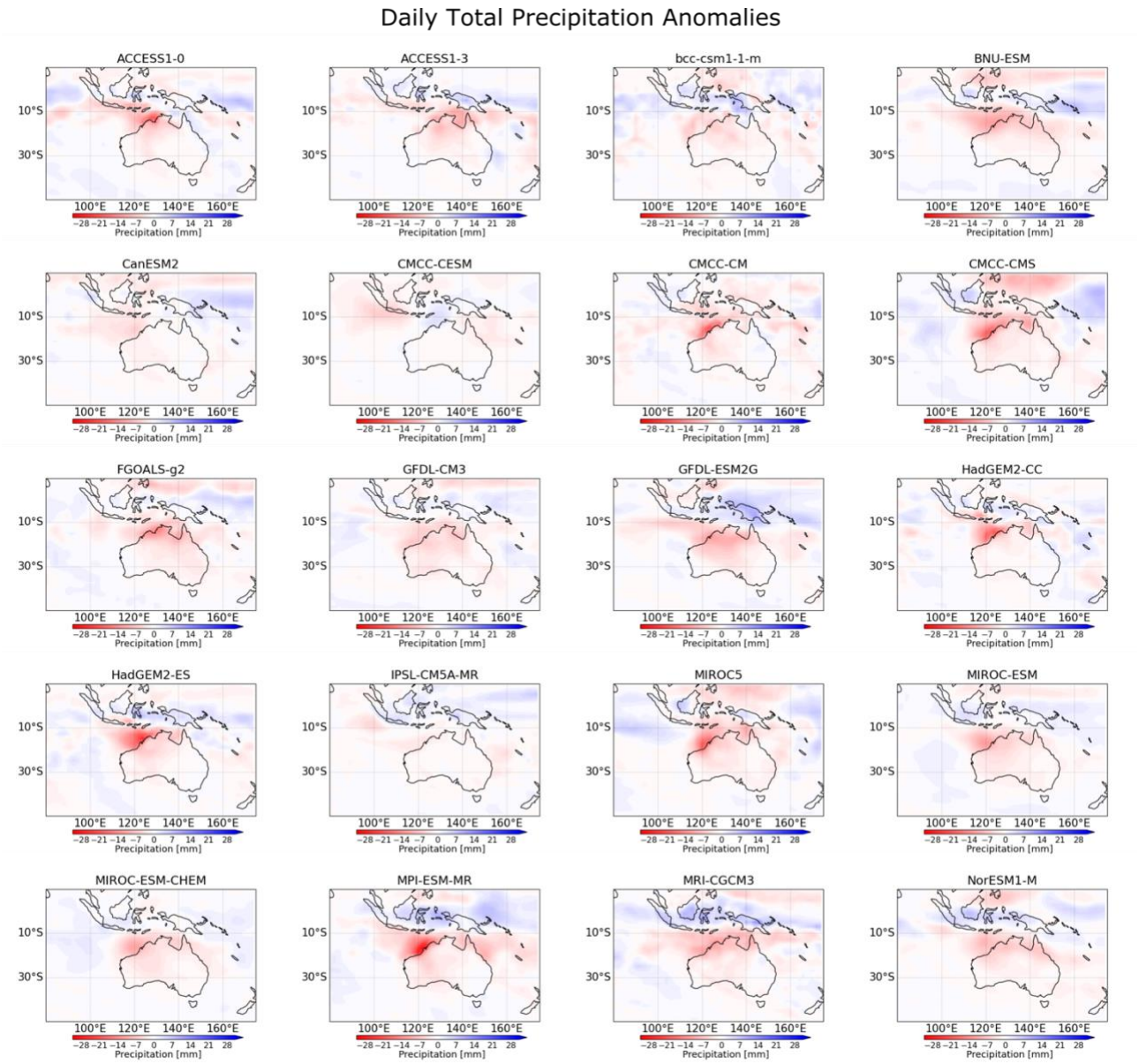

Figure 18 - Anomaly composites (strong-minus-no High days) of daily total rainfall (mm day^{-1}) for 20 CMIP5 historical simulations for March.

Figure 19 presents the relative frequency of dry days and highlights the intermodel variability. Ten of the models display the relationship between the High and dry day frequency very well, whereby a maximum increase in relative frequency of 20-40% is seen over the majority of Australia during stronger High days, and a small section on the south-west coast shows a decrease of approximately 20%. CanESM2, GFDL-CM3 and IPSL-CM5A-MR show an increase in relative frequency of 20-40%, but this is seen further south over the Australia landmass. None of the models show significantly stronger changes in relative frequency than ERA5, however, some show weaker changes. CMCC-CESM and CMCC-CM display a weaker increase over central Australia of 10% and a weaker decrease over the south-west coast of 5-10%.

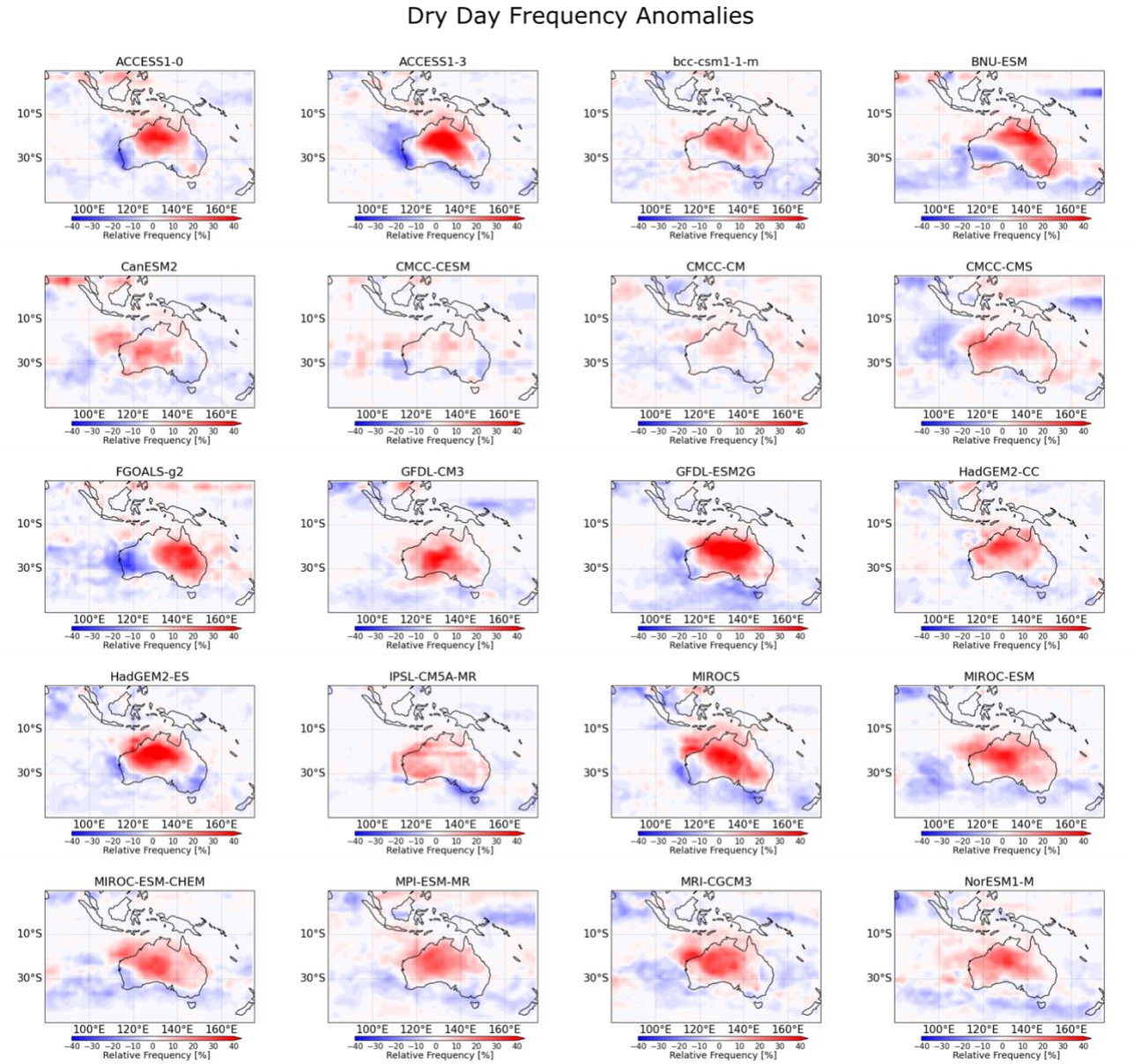

Figure 19 - Anomaly composites (strong-minus-no High days) of the relative frequency of extreme dry days for 20 CMIP5 historical simulations for March.

A more stringent test of models is in their ability to represent the relationship between heavy rainfall and the Bilybara High, due to the known deficiencies in the simulation of heavy rainfall in CMIP5 (Irving et al., 2012). Figure 20 shows that there is a range of model performance in reproducing this relationship. Seventeen of the models accurately represent the spatial distribution of the relationship, displaying decreases in relative frequency over north and north-west Australia and increases over the Maritime continent. However, almost all of the models overestimate this decrease in frequency by a significant amount. A maximum decrease of 60% is evident in MPI-ESM-MR, and there are also other significantly larger decreases than ERA5 seen in BNU-ESM, CMCC-CMS, HadGEM2-ES, MIROC-ESM and MIROC-ESM-CHEM that range between 35% and 55%. Alternatively, some models show little to no change in relative frequency over Australia. BCC-CSM1-1-m shows a much weaker maximum decrease in relative frequency of 15%, and CanESM2, CMCC-CESM and IPSL-CM5A-MR all present almost no change.

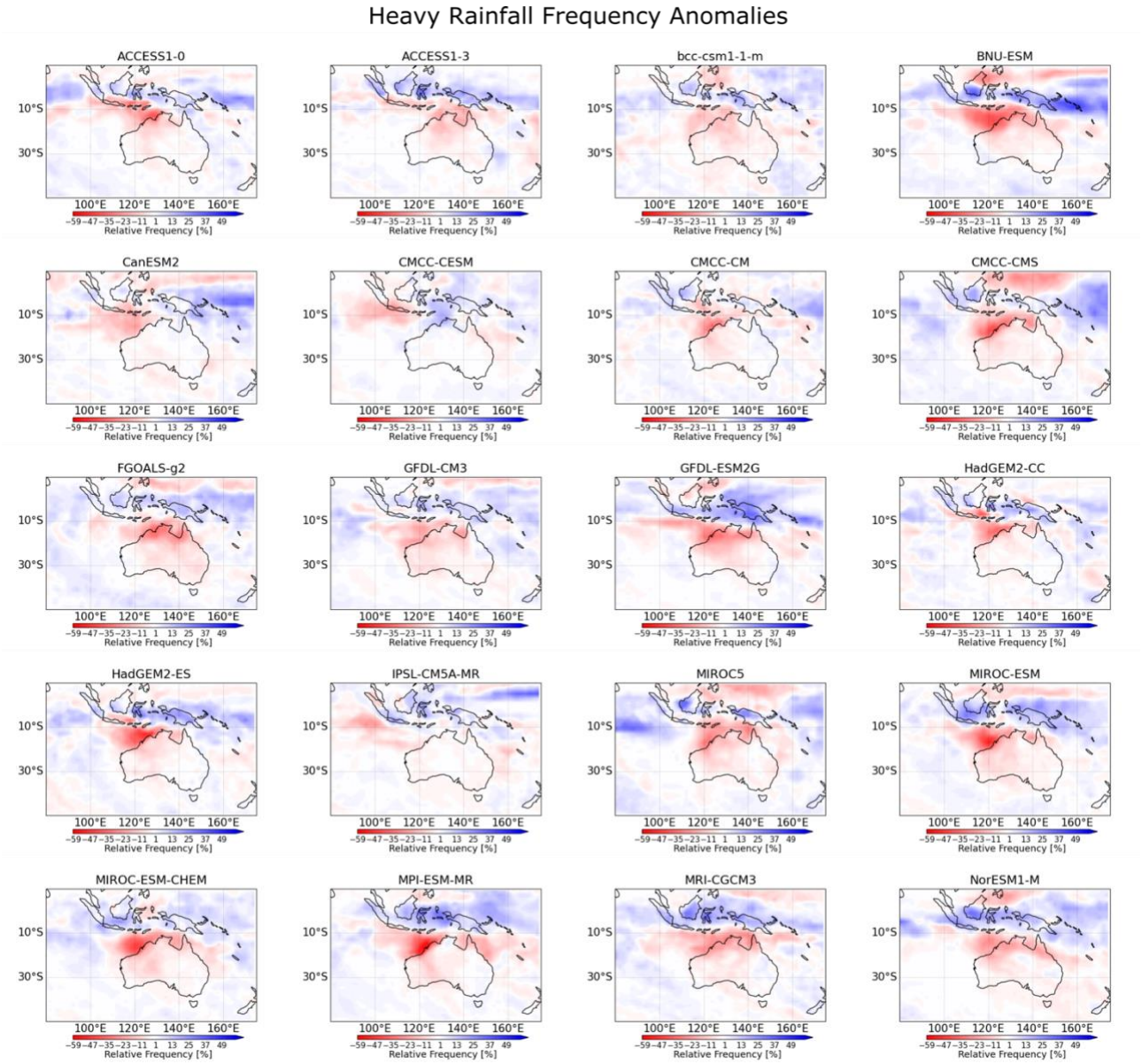

Figure 20 - Anomaly composites (strong-minus-no High days) of the relative frequency of extreme heavy rainfall days for 20 CMIP5 historical simulations for March.

Australian rainfall is often poorly represented in models (e.g., Irving et al., 2012), and thus it was not expected that Figures 18-20 would show completely accurate representations of the relationship between the Bilybara High and rainfall. The fact that the majority of models are able to show a reasonable relationship with mean rainfall composites is promising in regard to using these models to predict future changes. However, the relative frequency of extreme event plots were more varied, with a number of models not being able to represent the magnitude of the relationship with the High well. Furthermore, a handful of models completely lack the ability to represent the High and its relationships with rainfall means and extremes. These factors need to be taken into account when using the models for future projections.

4.2.2 Temperature

Section 3.2.2 showed that a stronger Bilybara High is associated with increased temperatures (with an increase of up to 7°C) over large areas of north-west Australia. Figure 21 demonstrates that models generally capture the relationship between a stronger High and increased temperature. Nine of the CMIP5 models assessed in this study perform extremely well in capturing this relationship confirmed using ERA5 data. These nine models have very similar spatial extents (approximately 4-5 million km^2 of the Australian landmass), and all show maximum increases in temperature of 4-6°C, with the highest increase being over approximately the area covered by the core region of the High. However, over half the models struggle to represent this relationship. CMCC-CESM, GFDL-CM3 and GFDL-ESM2G have much weaker increases in temperature, around 1-2°C, and are more southerly and centrally focused. FGOALS-g2 shows a 5-7°C temperature increase over the entirety of the Australian landmass rather than just the area to the north-west, and NorESM1-M has a similar spatial extent except with a weaker maximum temperature increase of 3°C. Thus, these two models overestimate the spatial scale of the High's influence. Eleven of the models also capture the area of temperature decrease on the south or south-east coast which is evident in the ERA5 plots. While a number of the models capture the relationship between the strength of the High and temperature very well, many of the model simulations vary in strength and spatial extent.

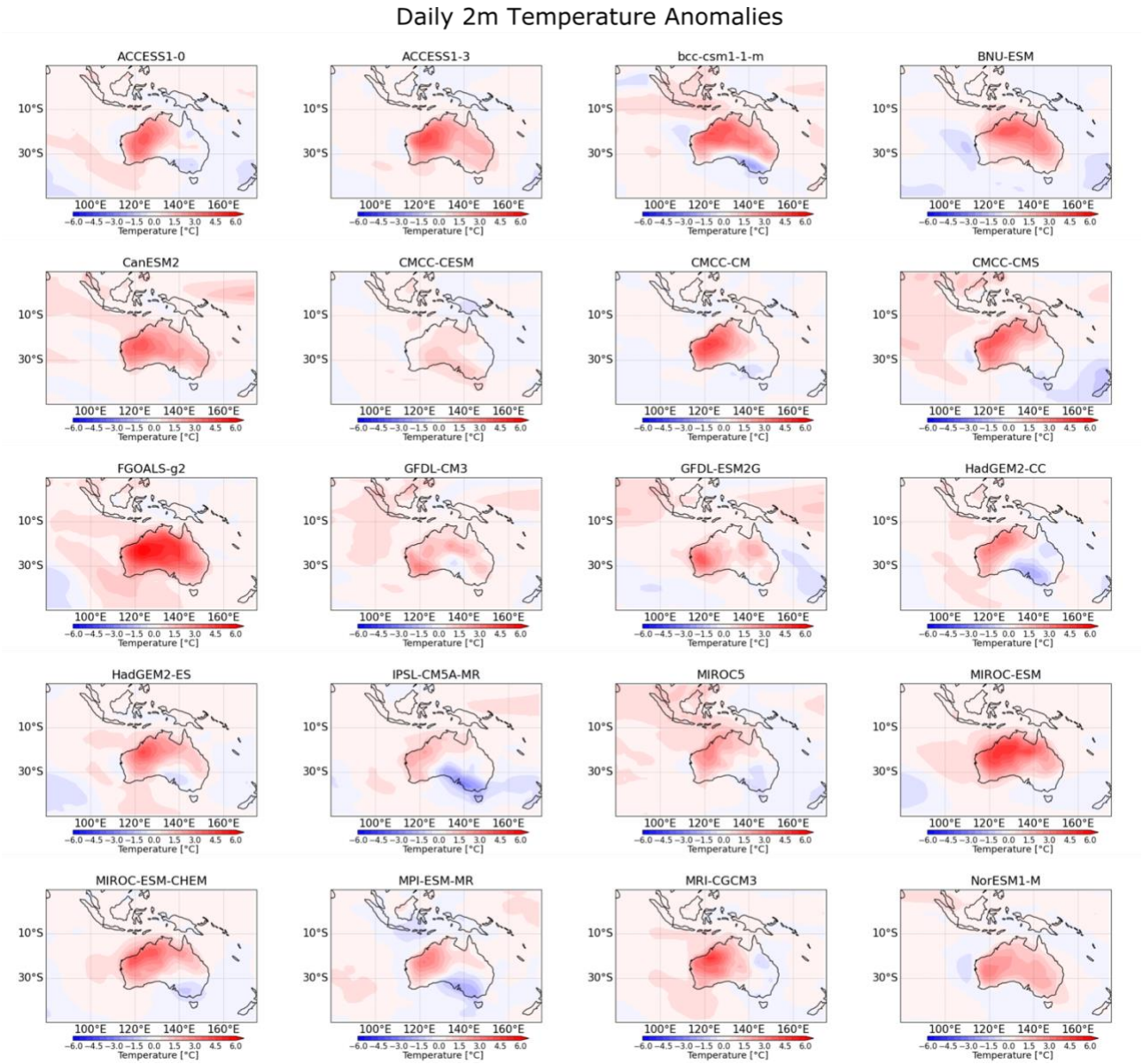

Figure 21 - Anomaly composites (strong-minus-no High days) of daily near-surface temperature (°C) for 20 CMIP5 historical simulations for March.

Figure 22 shows that a large number of the models are able to capture the relationship between the strength of the Bilybara High and extreme high temperature frequency, as demonstrated by the ERA5 data. This relationship shows that as the strength of the High increases, the relative frequency of extreme high temperature days increases by approximately 37% over a large area of north-west and central Australia, and this frequency decreases over a range of nearby ocean areas. While some models do not quite match this relationship, the majority only differ slightly. CanESM2, CMCC-CESM, GFDL-CM3, GFDL-ESM2G and IPSL-CM5A-MR show quite accurate spatial patterns, however, have weaker maximum increases in relative frequency than ERA5. These frequency increases range from 10-30%. Meanwhile, HadGEM2-CC, MIROC5 and MPI-ESM-MR show the correct magnitudes of change but on smaller spatial scales. Alternatively, FGOALS-g2 has a much

larger spatial extent that covers the majority of Australia and has a maximum anomaly increase of 48%, which is much higher than shown in ERA5.

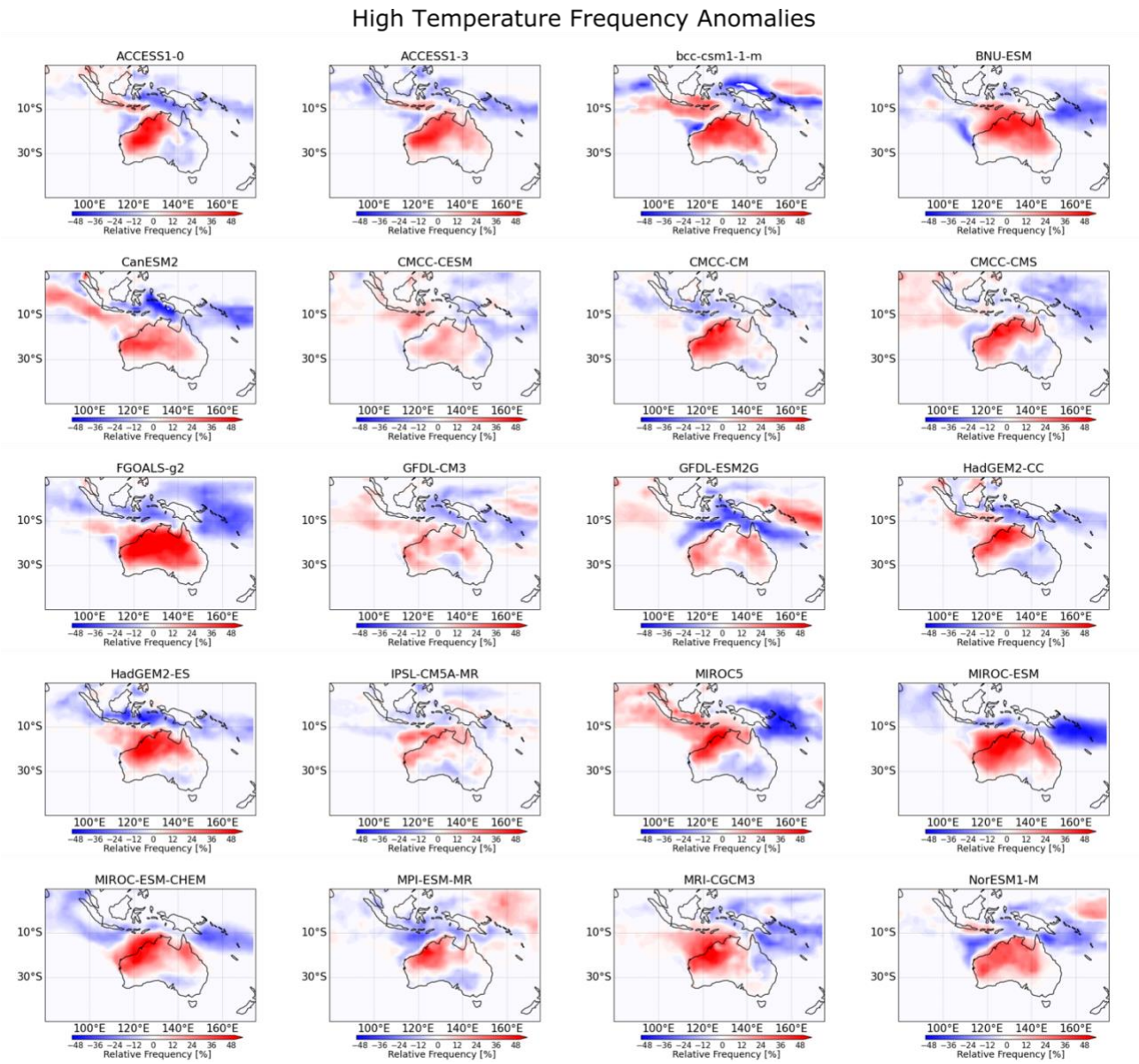

Figure 22 - Anomaly composites (strong-minus-no High days) of the relative frequency of extreme high temperature days for 20 CMIP5 historical simulations for March.

Overall, almost all models are able to capture the general positive relationship between the Bilybara High and temperature. However, over half the models struggle regarding the magnitude of change between strong and no High days as well as the spatial extents of the relationships.

4.3 Overview of CMIP5 representation of the High

This section has demonstrated that the CMIP5 models do represent the Bilybara High, and broadly we have shown that they simulate reasonable relationships between the High and rainfall and

temperature. The questions that follow these discoveries are whether similar relationships exist in future years (2075-2100) and whether intermodel variability in projections of the strength of the High is linked with intermodel variability in projections of rainfall and temperature.

Section 5: Future projections of the Bilybara High in CMIP5

The Bilybara High and its influence on rainfall and temperature are relatively faithfully reproduced in CMIP5 models under historical simulations. This gives some confidence that the same models can be used to assess the future changes in the Bilybara High and its influences on the climate. Hence, this section will address whether the Bilybara High can be captured in future simulations of 2075-2100 and whether the High remains important in the future in terms of daily rainfall and temperature means and extremes for March.

5.1 Future simulation of the High in CMIP5 models

For future projections of rainfall and temperature to be deemed useful, it is first important to determine whether the Bilybara High is present in future simulations. Figure 23 provides evidence that all the models, to some extent, show the high-pressure system over north-west Australia. The main difference between these future simulations compared to historical simulations is that the future simulations have a larger spatial area experiencing positive GPH anomalies between no High days and strong High days. Essentially, the same pattern can be seen as in historical simulations but at an exaggerated state. As expected, models vary in the maximum anomaly of the strength of the High. CMCC-CESM and MPI-ESM-MR show the strongest anomalies, with the centres of the High reaching maximum values of 98m. Meanwhile, BNU-ESM, CanESM2, FGOALS-g2, GFDL-ESM2G, IPSL-CM5A-MR, MRI-CGCM3 and NorESM1-M have weaker maximum anomaly values of 40-70m. These upper and lower maximum anomaly values are very similar to those seen in the historical model simulations, which suggests that in the future the GPH differences between no High days and strong High days remain largely similar. Also, a handful of models simulate an altered location of the High. ACCESS1-0, which has done well in capturing the High and its relationships thus far in historical simulations, projects the High at a more southward position in the future. This is also the case for HadGEM2-CC and IPSL-CM5A-MR. HadGEM2-CC also diverges from its historical output regarding the spatial extent of the High as the projected high-pressure system is stretched much further south to a latitude of almost 50°S. This indicates that in some models there is a possible southward extension or shift in the High.

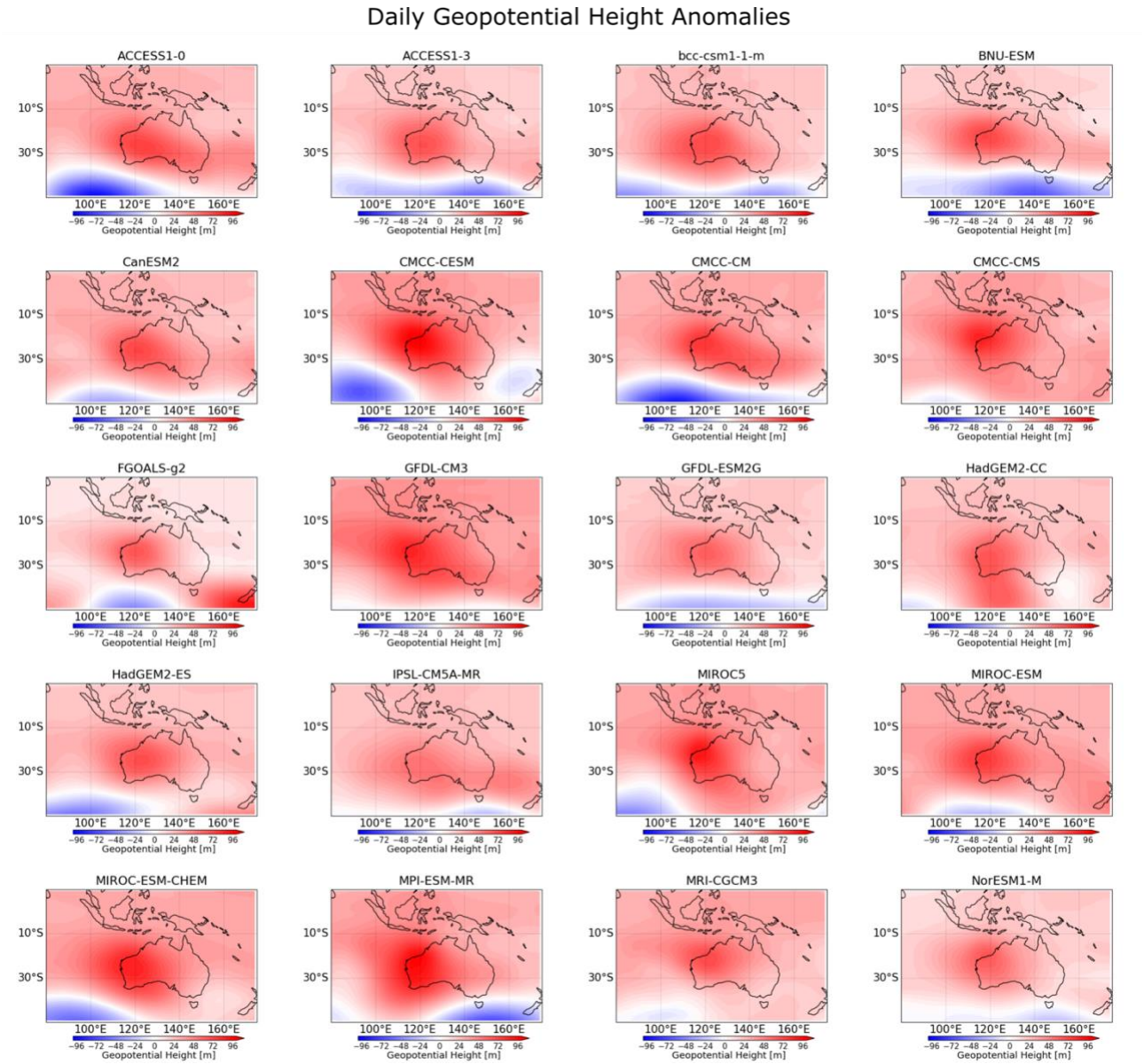

Figure 23 - Anomaly composites (strong-minus-no High days) of daily geopotential height (m) at 500hPa for 20 CMIP5 RCP8.5 simulations for March.

Figure 24 shows that almost all models have very similar strong High thresholds, which suggests that the strengths of the High see little change. For the most part, intermodel variation in simulation is much bigger than the magnitude of future change. The only significant changes are in CMCC-CESM, IPSL-CM5A-MR and MIROC-ESM, with the largest of these changes (MIROC-ESM) being taken into account in Section 6 of this study by being removed from statistical testing given also its severe overestimation of the strength of the High in the present day (Figure 17). Each model differs in whether the historical or future simulation has a higher threshold, with eight having higher future thresholds and twelve having higher historical thresholds, and thus no systematic directional change in the strength of the High can be determined.

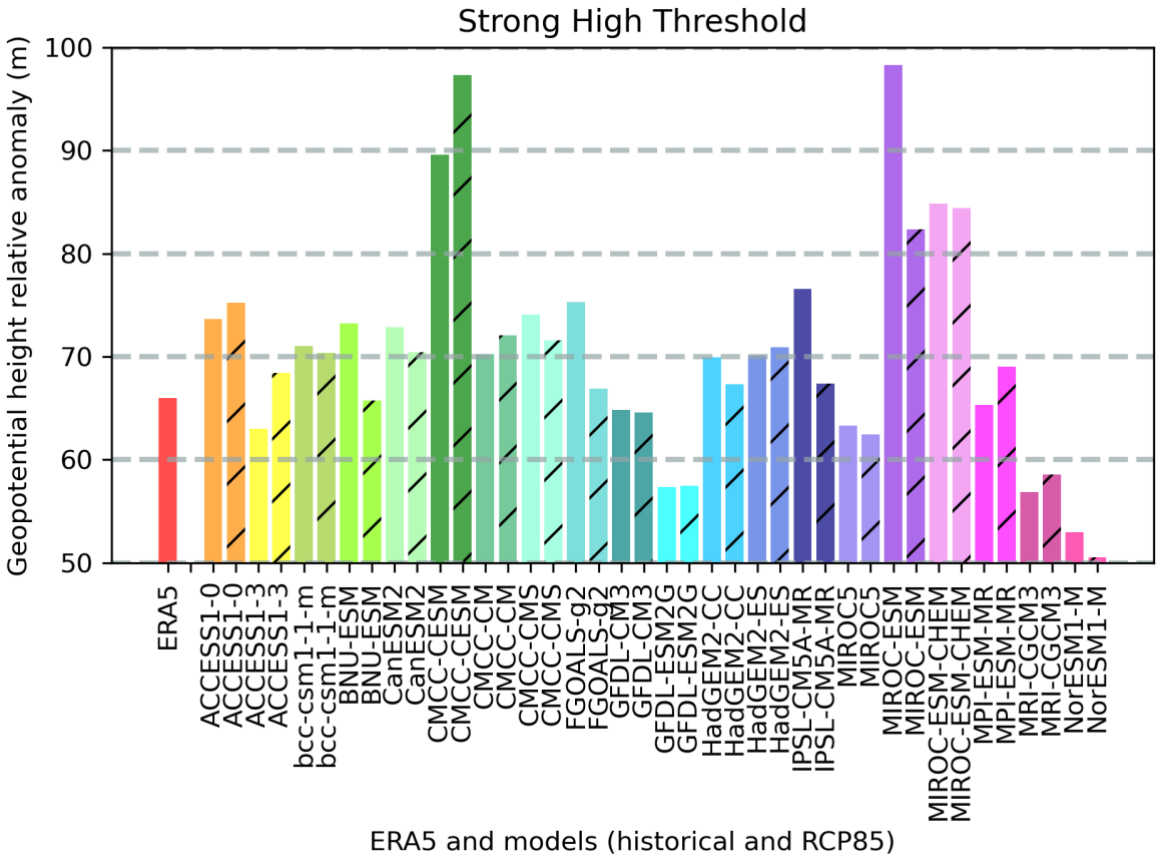

Figure 24 – A bar graph showing the strong High threshold (the 80th percentile of the Relative Anomaly High Index) for each model to compare the historical and future simulations for March. Historical simulations are shown by bars with block colours and future simulations are shown by bars with lines.

5.2 The relationship between the High and rainfall and temperature in 2075-2100

5.2.1 Rainfall

Figure 25 shows how mean rainfall composites will change as a result of the Bilybara High in the future. A large number of the models simulate very large decreases in total rainfall over north-west Australia on strong High days compared to no High days. Twelve models show rainfall decreases ranging from 15-28mm, with the largest decrease of 28mm being seen in the CMCC-CESM model. These magnitudes of change are generally similar to those seen in the historical simulations. ACCESS1-3 also predicts a large negative rainfall anomaly, but this does not completely follow the pattern seen in the other models or the historical simulations, as instead, it projects a decrease centred over a more north-eastward location and particularly over the Arafura Sea, rather than the usual north-west projection that extends over the Timor Sea. ACCESS1-0, CanESM2 and IPSL-CM5A-MR show very little difference in rainfall between strong and no High days over the Australian landmass. For ACCESS1-0, this does not coincide with the patterns seen in the respective historical simulation.

However, this does correspond with the CanESM2 and IPSL-CM5A-MR historical simulations which also show a very weak rainfall anomaly.

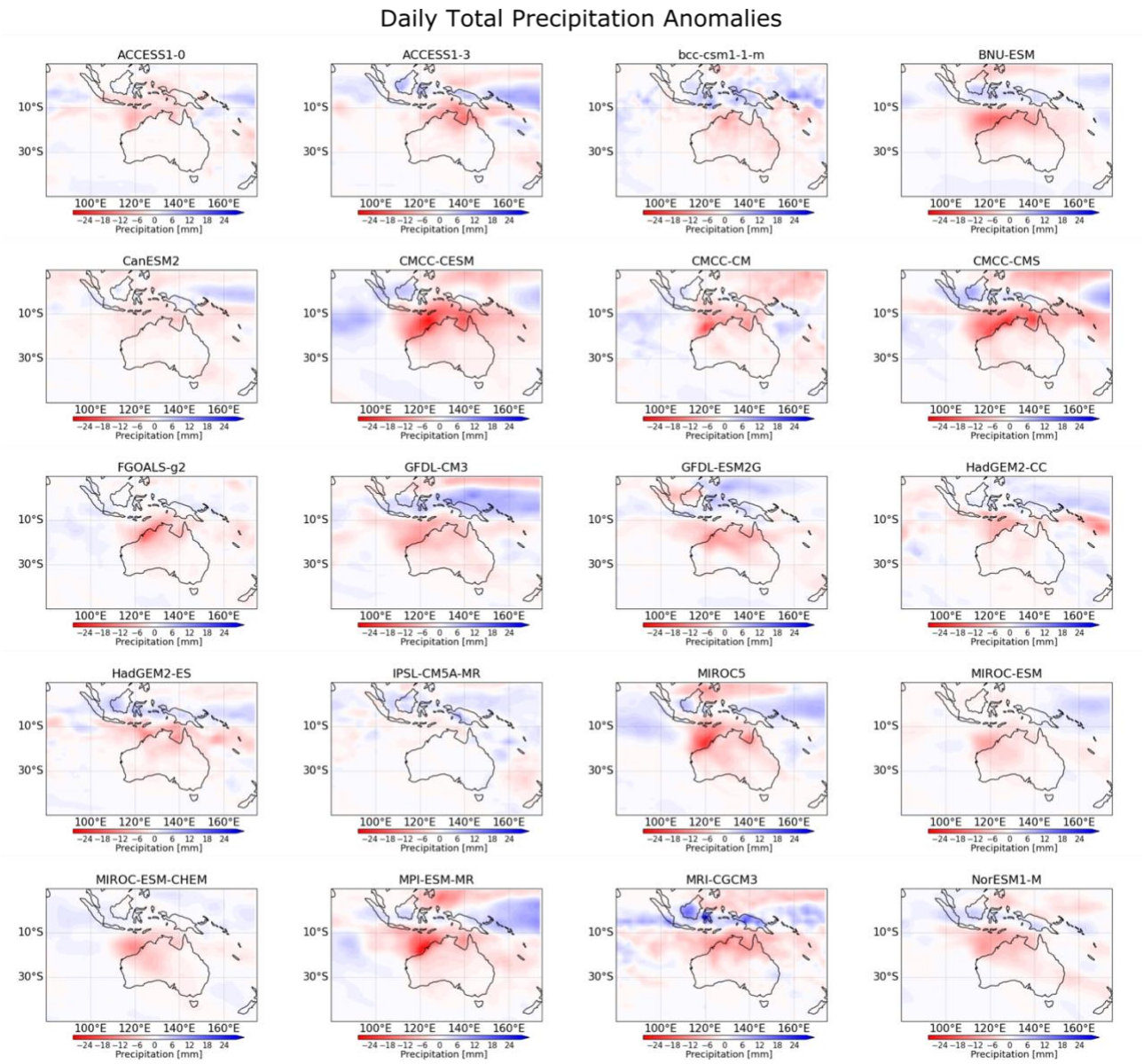

Figure 25 - Anomaly composites (strong-minus-no High days) of daily total rainfall (mm day^{-1}) for 20 CMIP5 RCP8.5 simulations for March.

Unexpectedly, Figure 26 shows that a number of the models show reasonably weak increases in the relative frequency of dry days on days with a strong High compared to those with no High in the future. ACCESS1-0, CanESM2, CMCC-CM, CMCC-CMS, MIROC-ESM and MPI-ESM-MR all show an increase in the relative frequency of dry days, but this increase is fairly small (maximum increases of 5-20%). This demonstrates that, for some models, the strength of the Bilybara High has less of an impact on dry day frequency than seen in historical simulations. Other models show patterns and strengths very similar to those seen in historical simulations, whereby a large area of north-west Australia sees an increase in dry day relative frequency of around 35%. The only model to show no

resemblance to the patterns seen in previous figures is IPSL-CM5A-MR, which captures a slight decrease in dry day frequency over some parts of central Australia for stronger High days. This is likely related to the weaker GPH anomaly, compared to other models, seen in Figure 23.

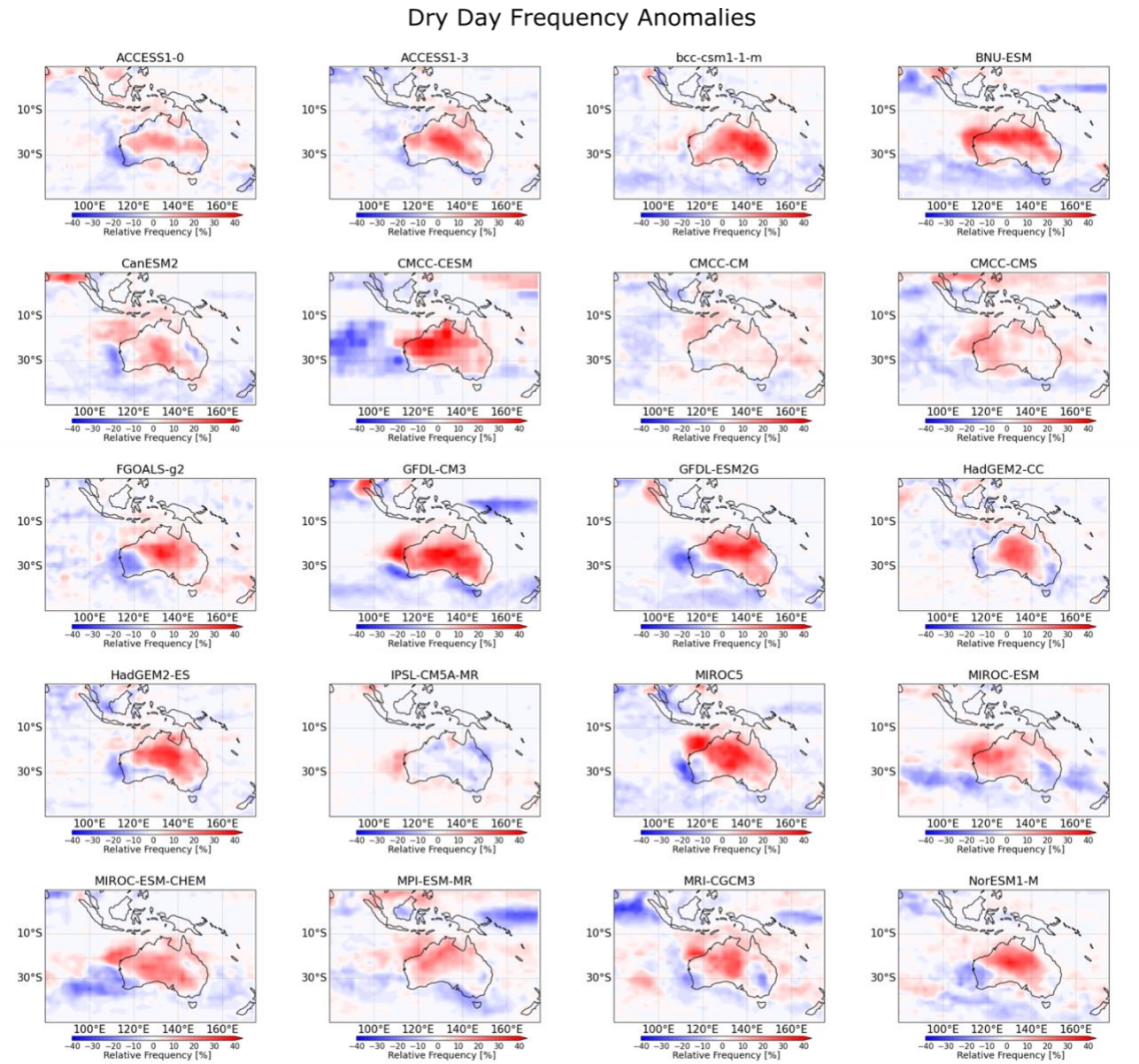

Figure 26 - Anomaly composites (strong-minus-no High days) of the relative frequency of extreme dry days for 20 CMIP5 RCP8.5 simulations for March.

The heavy rainfall relative frequency anomaly plots for RCP8.5 simulations in Figure 27 again show that models vary in comparison to historical simulations. Several models - BNU-ESM, CMCC-CESM, CMCC-CMS, MIROC5, MIROC-ESM-CHEM and MPI-ESM-MR – show a significant decrease in the relative frequency of extreme heavy rainfall for stronger High days, with maximum frequencies decreasing by as much as 71% over north-west Australia. However, some models show weak or no anomalies. BCC-CSM1-1-m, CMCC-CM, HadGEM2-CC and HadGEM2-ES have weak maximum decreases in frequency of 5-20% over the landmass. ACCESS1-0, CanESM2 and IPSL-

CM5A-MR have almost no difference in frequency over the landmass between no High days and strong High days. ACCESS1-0, CanESM2 and IPSL-CM5A-MR also struggled to show any change in rainfall composites (Figure 25), suggesting that these models struggle to accurately represent rainfall. Interestingly, analogous to Figure 25, ACCESS1-3 captures a negative anomaly over northeast Australia rather than the expected north-west.

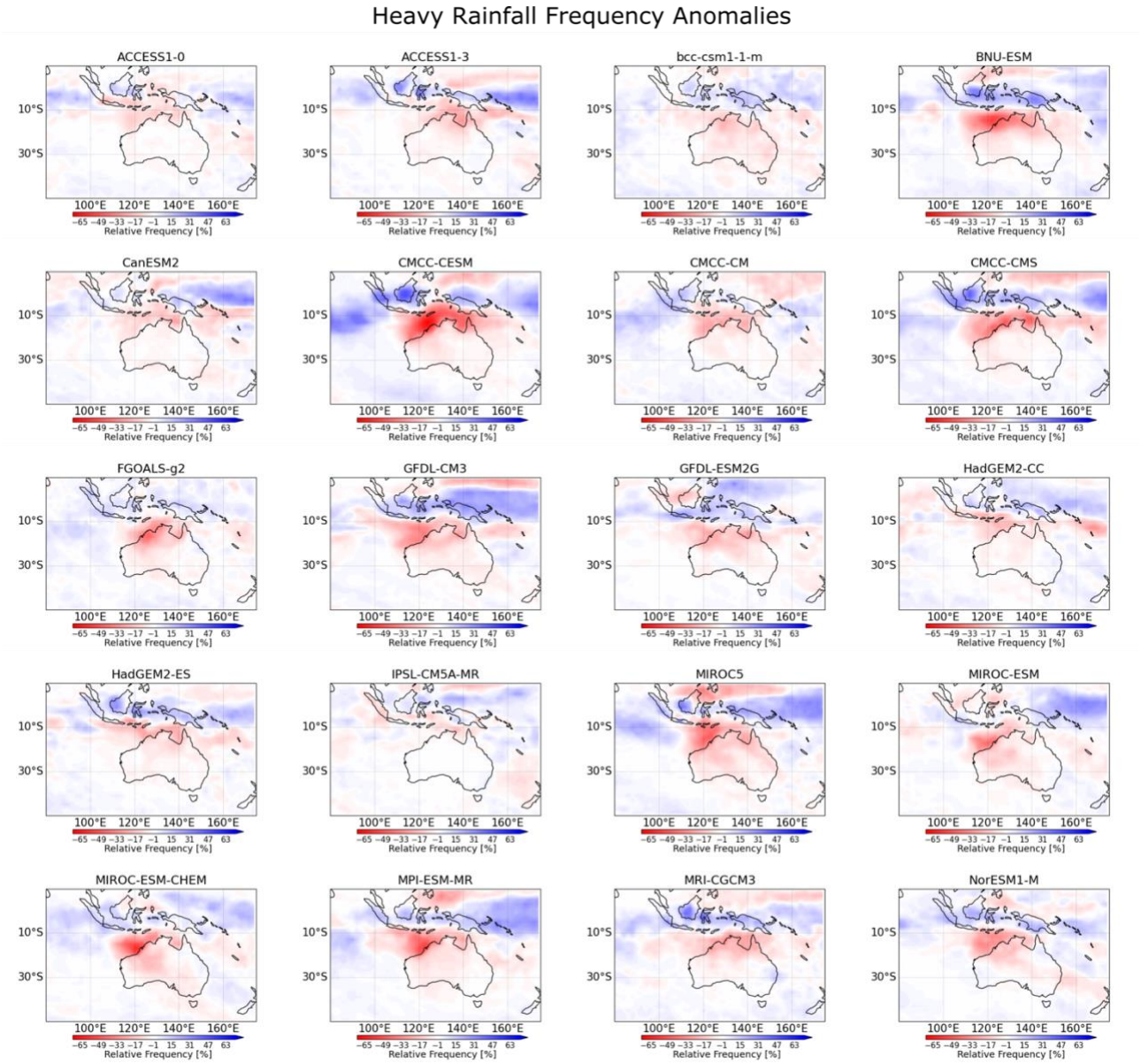

Figure 27 - Anomaly composites (strong-minus-no High days) of the relative frequency of extreme heavy rainfall days for 20 CMIP5 RCP8.5 simulations for March.

Because rainfall is often poorly represented in models, values often fluctuate significantly between models. Figure 28 shows the varying heavy precipitation thresholds for models and highlights the differences models have for rainfall simulations. Two models (FGOALS-g2 and MRI-CGCM3) are quite substantial overestimates of the ERA5 threshold: however, eleven models significantly underestimate it. Regarding differences between model historical and future simulations, thirteen of

the models have much higher future heavy rainfall thresholds, three have much higher historical thresholds, and four have little change. This demonstrates that in general, the threshold for heavy rainfall is increasing in the future, which is consistent with theoretical expectation (Min et al., 2011), but also that the level of uncertainty between models needs to be considered. Ultimately, this will notably affect the outcomes of the plots in Figures 25, 26 and 27 regardless of the effect of the High on rainfall levels.

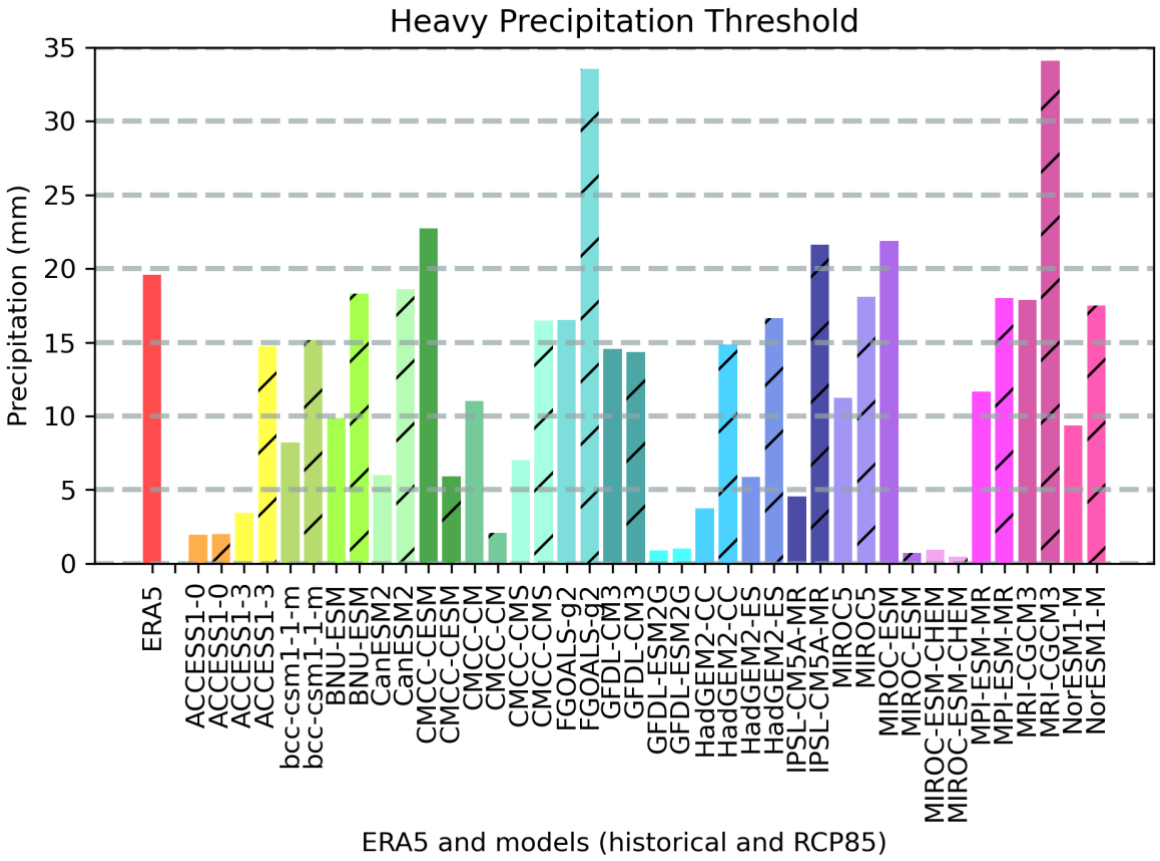

Figure 28 - A bar graph showing the heavy precipitation threshold (the 90th percentile of the daily rainfall) for each model to compare the historical and future simulations for March. Historical simulations are shown by bars with block colours and future simulations are shown by bars with lines.

5.2.2 Temperature

Looking at the anomaly between strong High days and no High days for temperature composites in Figure 29, it is clear that the stronger the Bilybara High, the higher the temperature increase occurring over a large area of north-west Australia. All models show this relationship very evidently. CMCC-CESM, GFDL-CM3 and MIROC-ESM-CHEM show the largest increases in temperature of 7°C. BCC-CSM1-1-m also shows a large temperature increase, however, this increase expands over a larger spatial scale of the whole Australian landmass (over 7.5 million km^2). This is also the case for GFDL-CM3 and MIROC-ESM-CHEM. Sixteen of the models have temperature increases across the

whole larger Australia region, which is less evident in historical simulations, with CMCC-CM, IPSL-CM5A-MR and MIROC-ESM-CHEM showing this most clearly. This maps onto the plots showing the larger spatial extent of the GPH anomaly in future simulations seen in Figure 23.

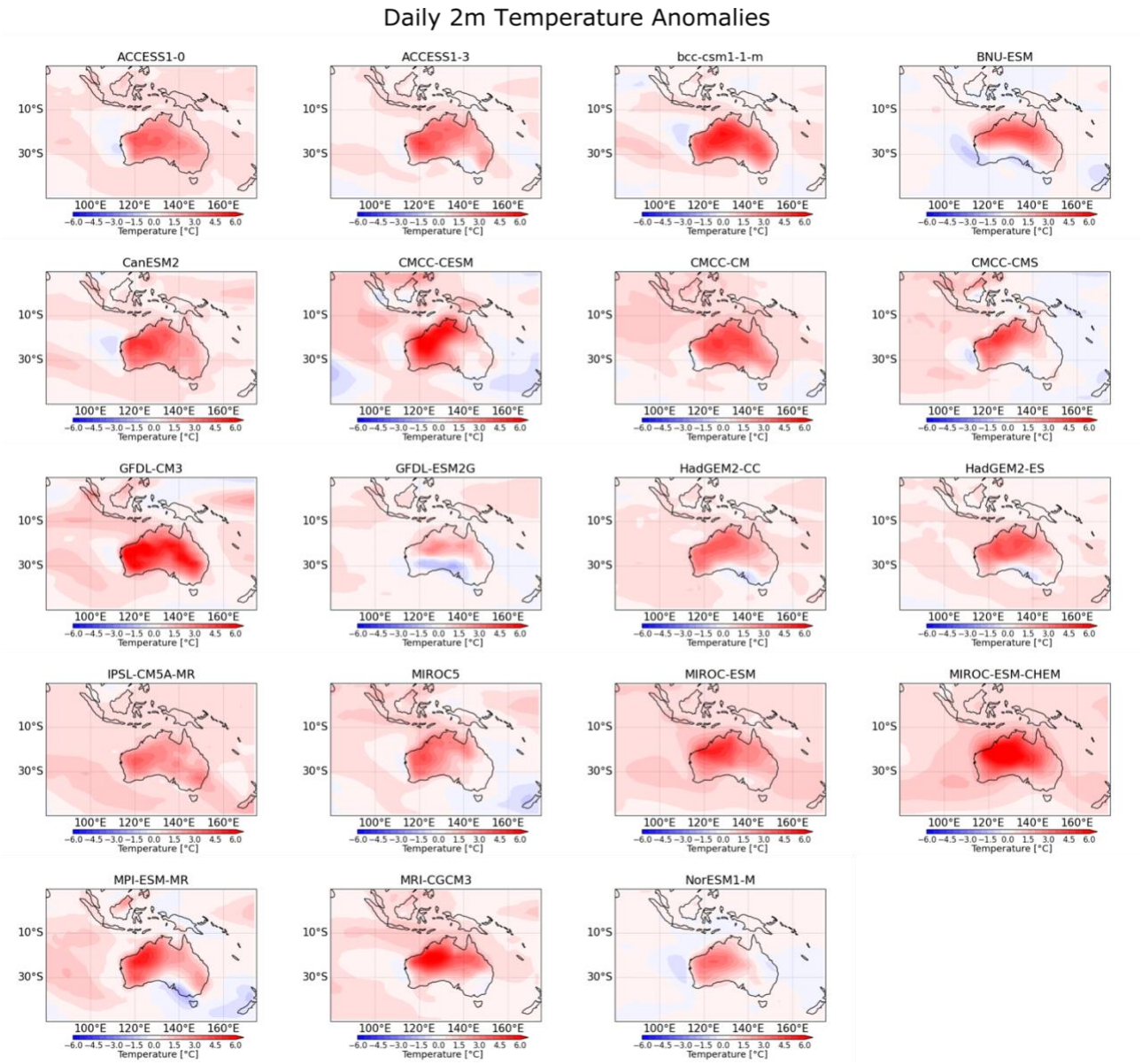

Figure 29 - Anomaly composites (strong-minus-no High days) of daily near-surface temperature (°C) for 20 CMIP5 RCP8.5 simulations for March.

Figure 30, showing anomalies for the relative frequency of high temperature days, shows models consistently capturing a very similar relationship to that seen using historical simulations. All models show a large increase in the frequency of high temperature days across almost all of the Australian landmass. The model with the strongest anomaly increase is CMCC-CESM which has a maximum increase of 62%. Meanwhile, IPSL-CM5A-MR displays the weakest increase in frequency, ranging from 0-15% across Australia. The models also manage to capture the decrease in frequency of high temperature days over the Maritime continent, with some models (e.g., CMCC-CMS and MIROC5)

also picking up decreases on the east and southeast coast. BNU-ESM and GFDL-ESM2G are the only models that arguably did not capture the relationship between the strength of the High and high temperature day frequency well. This is because, although a section of increased frequency is present over parts of northern Australia, areas of central-west Australia show a decrease in frequency of 10-20%, which no other models show.

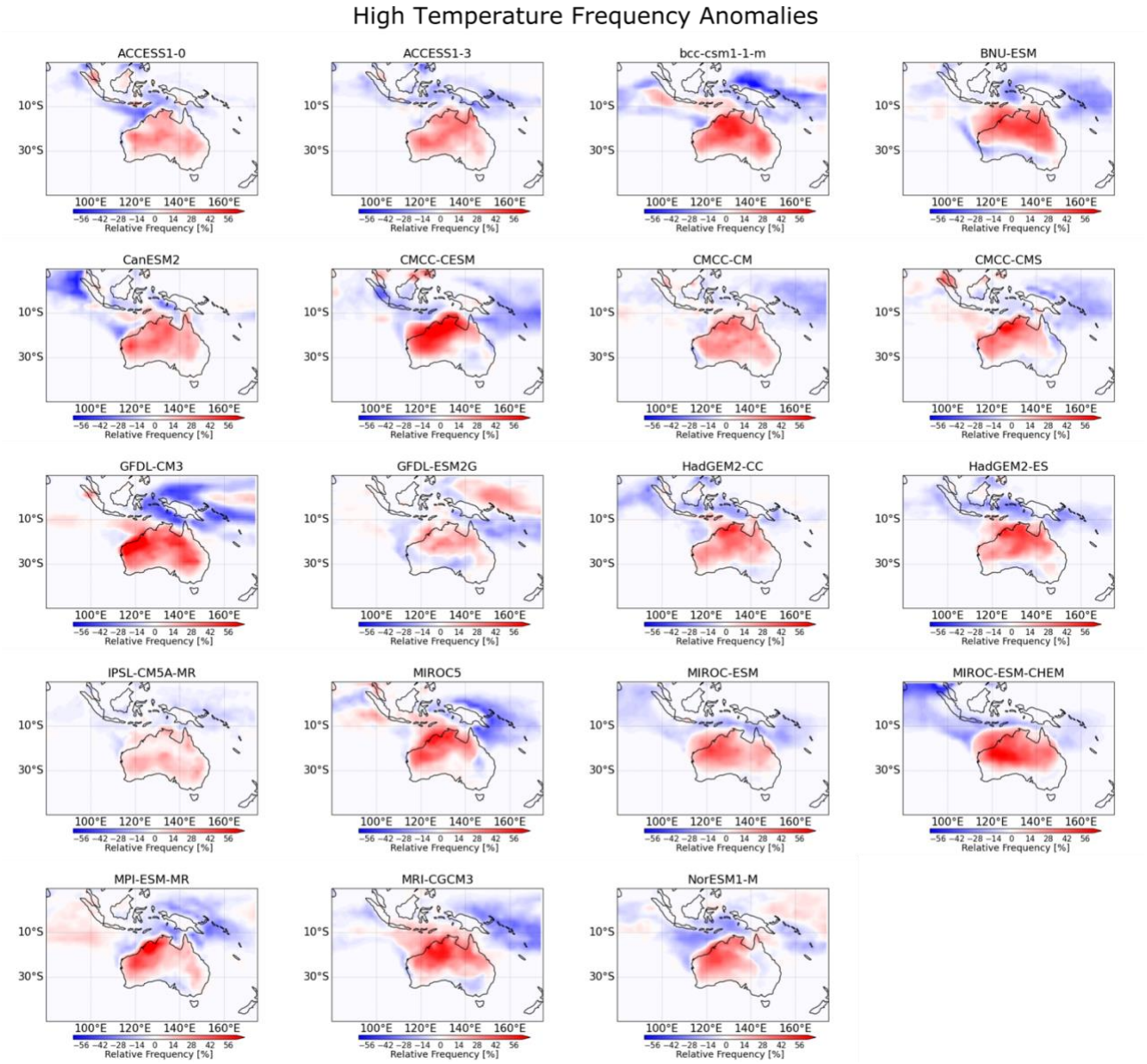

Figure 30 - Anomaly composites (strong-minus-no High days) of the relative frequency of extreme high temperature days for 20 CMIP5 RCP8.5 simulations for March.

5.3 Overview of CMIP5 future simulation representation of the High

The Bilybara High is present in future simulations of 2075-2100. These simulations also show that the High is still important in influencing mean and extreme rainfall and temperature in the future period, with similar relationships as seen in historical simulations being evident. Having said this, a

key difference is the larger spatial extent of the mean temperature anomalies, which is consistent between models and relates to the larger spatial extent of the High in future simulations. Also, the maximum anomaly values for high temperature and heavy rainfall frequencies are much larger in future simulations. This is important information for predicting future Australian climatology and for those planning adaptation strategies for future increases in the severity and frequency of drought conditions in Australia. Ultimately, Sections 4 and 5 of this study suggest that evaluating the intermodel variability in future projections of the Bilybara High could help to explain the spread of future projected rainfall and temperature. The results of this are discussed in the next section.

Section 6: Are future changes in the strength of the Bilybara High related to changes in rainfall and temperature among models?

Sections 4 and 5 have been carried out with the end focus of being able to project how intermodel differences in the changes to the Bilybara High will influence the spread of rainfall and temperature projections in the future. Examining both historical and future model simulations has shown that the models are generally able to capture the High and its relationships with rainfall and temperature to an extent that it is suitable to use these models for future projections. Scatter graphs have been produced (Figures 31 and 32) to determine how the strength of the Bilybara High is likely to change in the future compared to now, and how that change relates to changes in rainfall and temperature. This is assessed in terms of model variability: is intermodel variability in changes in the High related to intermodel variability in the changes in rainfall and temperature?

The key result, shown in Figure 31, is that there is a strong negative correlation between the variability in the model representation of the change in the strength of the Bilybara High and variability in the change in rainfall among models. This correlation is confirmed with a Pearson's Correlation Coefficient of -0.432 ($p<0.1$, $n=20$) when considering all model values, and a coefficient of -0.660 ($p<0.01$, $n=20$) when MIROC-ESM is removed. The step of removing MIROC-ESM from the correlation is sensible given its anomalously large GPH relative anomaly value for the historical simulation compared to its future simulation, evident in Figure 24, and its implausibly large strong High threshold relative to ERA5 (Figure 17). Overall, Figure 31 shows that the evolution of the Bilybara High is likely to be important in determining how much rainfall there is in the future. Models that have large increases in the strength of the High have relatively large decreases in rainfall, whereas models that project little change in the High show increases or little change in rainfall. The range of change in average daily rainfall is -2mm to 1.8 mm depending on how the strength of the High changes, which could have serious consequences for drought probability. Working out which of the futures displayed in Figure 31 is more probable will be important in helping to constrain what happens to rainfall in the future.

We also look at the correlation between variability in model representation of the strength of the High and variability in the change in temperature among models given that a stronger High is associated with higher temperatures on a daily timescale (Section 3.2.2). Figure 32 shows that there is no correlation ($r=-0.057$). There are many explanations for this, including that uncertainties in the future evolution of temperature at regional scales are dominated by global-scale uncertainties in equilibrium climate sensitivity and the transient climate response, including mixing uncertainties in the equatorial and sub-tropical radiative feedbacks (Proistosescu et al., 2020).

Scatter plots of the change in frequency of extreme dry days, heavy rainfall and high temperatures have also been produced (Appendix A), but again these show no significant correlations. This suggests that although the High clearly has an influence on extreme events in reanalysis and models (Sections 3, 4 and 5), average changes to the High do not scale with changes in extremes.

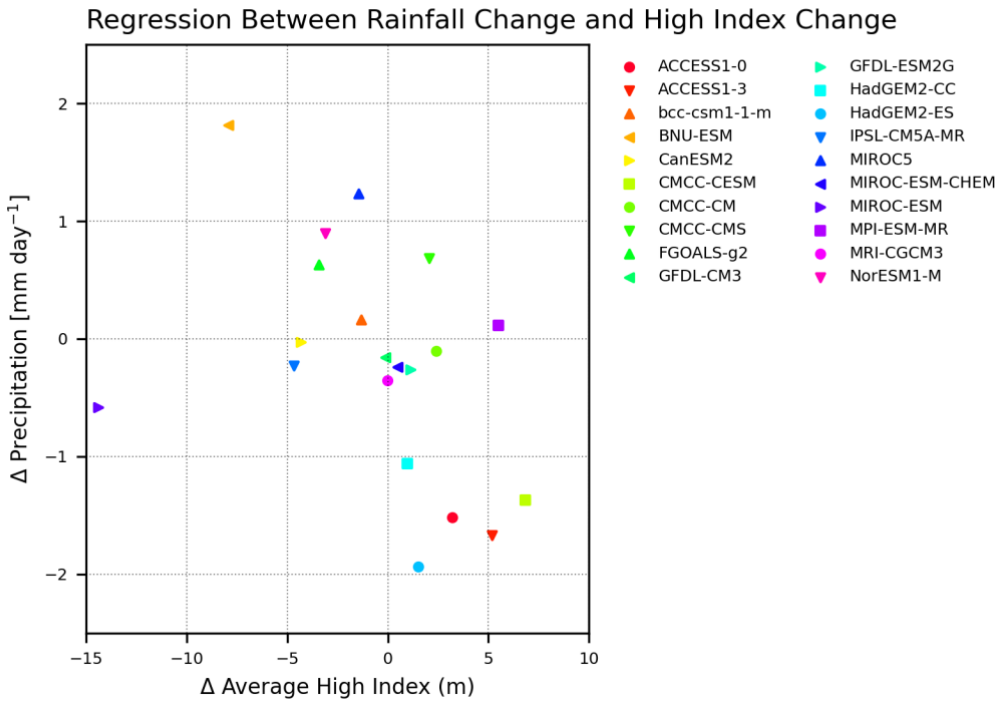

Figure 31 - To compare historical and RCP8.5 model data, a scatter plot has been produced. The plot shows changes in the average Relative Anomaly Index (m) on the x-axis and changes in daily precipitation (mm day^{-1}) on the y-axis. These changes were calculated by subtracting the area-averaged historical model datasets from the area-averaged RCP8.5 model datasets. The regions used for the area-averages can be seen in Figure 5.

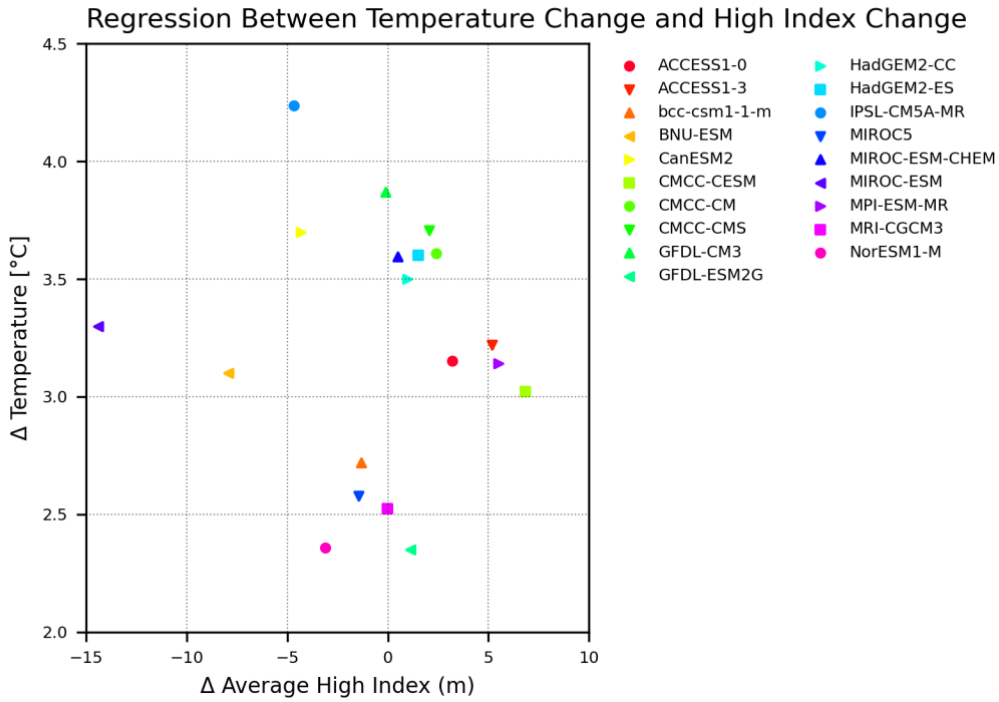

Figure 32 – The plot shows changes in the average Relative Anomaly Index (m) on the x-axis and changes in daily temperature (°C) on the y-axis. These changes were calculated by subtracting the area-averaged historical model datasets from the area-averaged RCP8.5 model datasets. The regions used for the area-averages can be seen in Figure 5.

Section 7: Conclusions

7.1 Summary of the main findings

The research undertaken in this study has presented novel results on how the Bilybara High impacts regional precipitation and temperature, both in the present day and in future projections. This section will summarise the main findings of the study in relation to each of the research questions presented in the introduction, as well as make suggestions for further research and present concluding remarks.

7.1.1 How does the Bilybara High impact rainfall and temperature in the high-resolution ERA5 reanalysis data?

Few studies have previously been conducted on the Bilybara High (Lenters and Cook, 1997; Reason 2016; Reason 2018). Research question 1 of this study aimed to build upon the coarse resolution NCEP reanalysis research undertaken by Reason (2018) that uses monthly mean values. This study has found that, using high-resolution ERA5 reanalysis data at daily timescales, the Bilybara High has a significant impact on regional rainfall and temperature over large areas of Australia. The results show that on days experiencing a strong High, rainfall can decrease by as much as 16mm (seen over north-western Australia) compared to days with no High identified. This suggests that the breakdown of the High is required for significant rainfall over north-western Australia. The results also show that on days experiencing a strong High, temperature can increase by as much as 7°C (seen over large areas of western Australia) compared to days with no High. These results provide general agreement with Reason (2018) but provide the evidence for the relationships between the High and rainfall and temperature at a higher resolution and using daily timescale data.

Question 1 of this study also extends upon the work by Reason (2018) to assess the impact of the Bilybara High on extreme climatologies. Results show a maximum increase of 38% in the frequency of extreme dry days, a maximum increase of 37% in the frequency of high temperature days, and a maximum decrease of 34% in the frequency of extreme heavy rainfall days when there is a strong High present compared to no High. These changes are seen over areas of northern and western Australia, with the Bilybara High having a limited impact on south-eastern Australia.

7.1.2 How is the Bilybara High and its relationships with rainfall and temperature represented in historical (1980-2005) CMIP5 simulations?

Research question 2 evaluates the representation of the Bilybara High in historical (1980-2005) simulations of the CMIP5 models. Overall, the models are able to capture the presence of the High, and its relationships with rainfall and temperature are generally well captured. Thirteen of the models underestimate the strength of the High and seven overestimate it compared to ERA5. Ten of the models display the relationship between the High and dry day frequency very well, with maximum increases of 20-40% being seen over the majority of the Australian landmass. Meanwhile, seventeen of the models accurately represent the spatial distribution of the relationship with heavy rainfall frequency, but almost all overestimate the decrease in frequency significantly compared to ERA5, with a maximum decrease of 60% being evident in MPI-ESM-MR. Nine models perform extremely well in capturing the relationship between the High and mean temperature which is displayed using ERA5 data, showing similar spatial extents and maximum increases of 4-6°C. Similarly, models are generally able to capture the relationship with extreme high temperature frequency shown using ERA5 data, but with some disparities in the magnitude of change and spatial extents. Overall, almost all of the models are able to capture the general relationships between the Bilybara High and rainfall and temperature as seen in ERA5 data, but inconsistencies emerge regarding the magnitude of change and spatial extents of the relationships.

7.1.3 How is the Bilybara High and its relationships with rainfall and temperature represented in future (2075-2100) CMIP5 simulations?

Research question 3 investigates the future (2075-2100) simulations. Overall, the Bilybara High is present in future simulations, and these simulations also show that the High is still important in influencing mean and extreme rainfall and temperature in the future period, with similar relationships as seen in historical simulations being evident. Comparing historical simulations to future simulations, eight models show the High is stronger in the future, and twelve show the High is weaker in the future. Furthermore, a key difference between historical and future simulations is that the future simulations have a larger spatial extent of maximum mean temperature anomalies, covering approximately the whole Australian landmass (over 7.5 million km^2) in the future compared to mainly the north and west of Australia (approximately 4-5 million km^2) in historical simulations. This is consistent between models and relates to the fact that the area outside the core region of the High, spanning the entire Australian landmass, increases in GPH anomaly from approximately 35m in historical simulations to 50m in future simulations. This increase in the spatial extent of high temperatures coincides with findings from Mukherjee and Mishra (2020) that show an increase in the

spatial extents of heatwaves with contemporary climate change. Additionally, when comparing strong High days to no High days, we find the maximum relative frequency of extreme high temperature days increases from 48% to 62% from historical to future model simulations. Similarly, the relative frequency of extreme heavy rainfall days decreases from -60% to -71%. Therefore, the results show an increase in extreme weather events in the future.

Moise et al. (2015) conclude that most CMIP5 models are able to represent the main features of the Australian climate. Meanwhile, other previous literature highlights some large biases in rainfall and temperature projections of the finer elements of the regional climate, especially regarding extremes (e.g., Alexander and Arblaster, 2017). This study concurs with Moise et al. (2015) in showing that CMIP5 models generally represent the Bilybara High and its relationships with rainfall and temperature in March well.

7.1.4 How does the Bilybara High change in the future compared to now, and how does that relate to changes in rainfall and temperature?

Given that models, in general, were able to reproduce the High and its relationship with rainfall and temperature, Section 6 considers how intermodel differences in the changes to the strength of the Bilybara High between historical and future simulations influences the spread of future projected rainfall and temperature. The results of this are presented in research question 4. The key result is that there is a strong negative correlation ($r = -0.660$, $p<0.01$, $n=20$) between variability in the model representation of the change in the strength of the Bilybara High and variability in the change in rainfall among models. This means that the evolution of the Bilybara High is likely to be significant in determining rainfall in the future, with models projecting big increases in the strength of the High also projecting relatively large decreases in mean rainfall. Previous literature has emphasised the uncertainties in rainfall change (e.g., Irving et al., 2012; Smith et al., 2012; Moise et al., 2015), for example, those related to patterns of SST change (Brown et al., 2016), and this result shows that this rainfall change is related in part to the Bilybara High. Conversely, there is no correlation between changes in the High and changes in mean temperature, or changes in the frequencies of extreme dry days, heavy rainfall days or high temperature days. An explanation for no correlation with temperature is likely to be that uncertainties in the future evolution of temperature at regional scales are dominated by global uncertainties in equilibrium climate sensitivity and the transient climate response (Proistosescu et al., 2020). Meanwhile, no correlations between extremes suggest that average changes to the High do not scale with changes in extremes.

7.1.5 Overview of findings

This study has shown that the Bilybara High has significant influences on regional precipitation and temperature, both in the present day and future projections. In the present day, a stronger High is linked with reduced rainfall, higher temperatures and increased temperature extremes over large parts of Australia. For the most part, models that project a strengthening High project reduced rainfall over Australia, while those with weaker Highs in the future project increasing rainfall.

This study advances the science focused on understanding local circulation features and the associated impacts on regional climates, and develops the broader body of literature evaluating the processes associated with climate changes. It does this by showing clearly that intermodel uncertainty in CMIP5 rainfall projections is linked with a regional circulation feature that we do not yet know much about, providing a key target for future research. The study has also demonstrated the importance of climate models in predicting future regional climate variables, as well as the weaknesses of models in representing regional features such as the Bilybara High.

7.2 Avenues for future research

The results presented have contributed to our understanding of the Bilybara High and its influence on regional rainfall and temperature over Australia, both in the present day and in future projections. However, further investigation is required to answer questions that were beyond the remit of this study. This study focuses only on March as that is when the Bilybara High is at its maximum strength. Future research could investigate the High and its relationships at other points in the annual cycle to assess how such relationships change. Furthermore, Reason (2016, 2018) considers the High on decadal timescales, but only with coarse resolution reanalysis data. As Section 3 of this study does, such decadal investigation could be undertaken using high-resolution reanalysis such as ERA5.

A systematic review of how the Bilybara High is represented across a range of datasets, including reanalysis and models, will clarify the results from this study. In particular, the newly available CMIP6 data should be investigated for future projections. Analysis of reanalysis and model data should also be complemented with in situ and direct observations. Investigating the High using a range of datasets will add robustness to the quantitative relationships uncovered in this study.

The Bilybara High is one of the mid-level high-pressure systems that has been identified in the Southern Hemisphere subtropics. Further work should look to understand the dynamics underlying

the High. For example, Figure 3 suggests there is some level of interaction with a heat low and convection over the Maritime continent, but the process by which this happens is not clear. It is important to investigate and understand because it is likely to aid climate science in other regions, and it will help with the issue of future climate prediction.

7.3 Concluding remarks

This study is important for governments and policymakers who must prepare and adapt for future regional climate changes in Australia. Providing climatic understanding to predict future weather patterns over large parts of north-west Australia is increasingly important with regards to the associated social and environmental impacts. The link between the Bilybara High and present-day extremes, including the UTCI which is relevant for human health, is important as it shows that successfully predicting the strength of the High on seasonal scales could aid preparedness for drought and heatwave events. In the future the temperature anomalies linked with the High are more spatially extensive, suggesting a wider impact on Australia, and extreme high temperature days are more frequent. Among many other impacts, this is likely to affect the magnitude and frequency of wildfires, which are detrimental to society and the environment (Dowdy et al., 2019). Drought conditions can also affect the livelihoods of those who work in the agricultural sector as crops often suffer in such conditions (Sharples et al., 2016). The results of this study provide policymakers with a more in-depth view of such extremes in the month of March and allow for more pre-planned and effective adaptation strategies.

References

Alexander, L. and Arblaster, J. (2017) Historical and projected trends in temperature and precipitation extremes in Australia in observations and CMIP5. *Weather and Climate Extremes*, 15, pp.34-56.

Arriagada, N. et al. (2019) Climate change, wildfires, heatwaves and health impacts in Australia. *Springer International Publishing*, pp.99-116.

Ashe, B. et al. (2009) Total cost of fire in Australia. *Journal of Risk Research*, 12(2), pp.121-136.

Brown, J. R. et al. (2010) An evaluation of rainfall frequency and intensity over the Australian region in a global climate model. *Journal of Climate*, 23(24), pp.6504–6525.

Brown, J. R. et al. (2016) Will a Warmer World Mean a Wetter or Drier Australian Monsoon? *Journal of Climate*, 29(12), pp.4577-4596.

Bureau of Meteorology (2008a) Climate of Australia. Bureau of Meteorology, Melbourne, p.214.

Climate Change in Australia (2016). Available at: https://www.climatechangeinaustralia.gov.au/en/climate-campus/climate-system/australian-climate-influences/ [Accessed: 18 August 2020].

Cook, B. I. et al. (2014) Global warming and 21st century drying. *Climate Dynamics*, 43(9-10), pp.2607-2627.

Dowdy, A. J. et al. (2019) Future changes in extreme weather and pyroconvection risk factors for Australian wildfires. *Nature Publishing Group*, 9(1), pp.1–11.

Driver, P. and Reason, C. J. C. (2017) Variability in the Botswana High and its relationships with rainfall and temperature characteristics over southern Africa. *International Journal of Climatology*, 37, pp. 570–581.

ECMWF (2020) ERA5. Available at: https://www.ecmwf.int/en/forecasts/datasets/reanalysis-datasets/era5 [Accessed: 14 September 2020].

Edwards, B. et al. (2018) The social and economic impacts of drought. *Australian Journal of Social Issues*, 54, pp.22-31.

Gallant, A.J. et al. (2018) Perceptions of thermal comfort in heatwave and non-heatwave conditions in Melbourne, Australia. *Urban Climate,* 23, pp.204-218.

Gergis J, et al. (2012) On the long-term context of the 1997–2009 'Big Dry' in south-eastern Australia: insights from a 206-year multi-proxy rainfall reconstruction. *Climate Change,* 111(3), pp.923–944.

Gibson, P. B., et al. (2017) Comparing Australian heat waves in the CMIP5 models through cluster analysis. *Journal of Geophysical Research: Atmospheres*, 122, pp.3266–3281.

Hersbach, H. et al. (2020) The ERA5 global reanalysis. *Quarterly Journal of the Royal Meteorological Society*, 146(730), pp.1999-2049.

Hopkins, A. J. M, et al. (2018) Forest die-off following global-change-type drought alters rhizosphere fungal communities. *Environ. Res. Lett*., 13.

Howard, E. and Washington, R. (2020) Tracing Future Spring and Summer Drying in Southern Africa to Tropical Lows and the Congo Air Boundary. *Journal of Climate, American Meteorological Society,* 33(14), pp.6205–6228.

IPCC (2012) Managing the Risks of Extreme Events and Disasters to Advance Climate Change Adaptation. A Special Report of Working Groups I and II of the Intergovernmental Panel on Climate Change. Cambridge University Press, Cambridge, UK, and New York, NY, USA, 582 pp.

IPCC (2013) The Physical Science Basis. Contribution of Working Group I to the Fifth Assessment Report of the Intergovernmental Panel on Climate Change. Cambridge University Press, Cambridge, United Kingdom and New York, NY, USA, 1535 pp.

Irving, D. B. et al. (2012) Climate projections for Australia: a first glance at CMIP5. *Australian Meteorological and Oceanographic Journal,* 62, pp.211-225.

James, R. et al. (2015): Process-based assessment of an ensemble of climate projections for West Africa. *Journal of Geophysical Research: Atmospheres,* 120, pp.1221-1238.

Kampmann, B. et al. (2013) An introduction to the universal thermal climate index (UTCI). *Geographia Polonica*, 86(1), pp.5-10.

Kirono, D. G. C, et al. (2020) Drought projections for Australia: Updated results and analysis of model simulations. *Weather and Climate Extremes*, 30.

Knutti, R. and Sedláček, J. (2013) Robustness and uncertainties in the new CMIP5 climate model projections. *Nature Climate Change*, 3, pp.369–373.

Lenters, J. D. and Cook, K. H (1997) On the Origin of the Bolivian High and Related Circulation Features of the South American Climate. *Journal of the Atmospheric Sciences*, 54 (5), pp.656-678.

Lim, E.-P. et al. (2016) Interaction of the recent 50-year SST trend and La Niña 2010: amplification of the Southern Annular Mode and Australian springtime rainfall. *Climate Dynamics*, 47, pp.7–8.

Lim, E.-P. et al. (2019) Australian hot and dry extremes induced by weakening of the stratospheric polar vortex. *Nature Geoscience*, 12, pp.896-901.

Marshall, AG. (2003) Trends in the Southern Annular Mode from observations and reanalyses. *Journal of Climate*, 16(24), pp.4134-4143.

Marshall, AG. et al. (2014) Intra-seasonal drivers of extreme heat over Australia in observations and POAMA-2. *Climate Dynamics*, 43(7), pp.1915–1937.

Matusick, G. et al. (2016) Eucalyptus forest shows low structural resistance and resilience to climate change-type drought. *Journal of Vegetation Science*, 27(3), pp.493-503.

Meneghini, B. et al. (2007) Association between Australian rainfall and the Southern Annular Mode. *International Journal of Climatology*, 27(1), pp.109-121.

Min, SK., et al. (2011) Human contribution to more-intense precipitation extremes. *Nature*, 470, pp.378–381.

Moise, A. et al. (2015) Evaluation of CMIP3 and CMIP5 Models over the Australian Region to Inform Confidence in Projections. *Australian Meteorological and Oceanographic Journal,* 65(1), pp.19-53.

Mukherjee, S., and Mishra, A. K. (2020) Increase in compound drought and heatwaves in a warming world. *Geophysical Research Letters*, 47.

Power, S. et al. (1999) Inter-decadal modulation of the impact of ENSO on Australia. *Climate Dynamics*. Springer, 15(5), pp.319–324.

Proistosescu, C. et al. (2020) Equilibrium climate sensitivity controls uncertainty in regional climate change over the 21st century. *OSF*, pp.1-7.

Reason, C. J. C. (2016) The Bolivian, Botswana, and Bilybara Highs and Southern Hemisphere drought/floods. *Geophysical Research Letters*, 43(3), pp.1280–1286.

Reason, C. J. C. (2018) Variability in rainfall over tropical Australia during summer and relationships with the Bilybara High. *Theoretical and Applied Climatology*, 132(1–2), pp.313–326.

Risbey, J. S. et al. (2009) On the Remote Drivers of Rainfall Variability in Australia. *Monthly Weather Review*, 137(10), pp.3233–3253.

Sharples, J. J. et al. (2016) Natural hazards in Australia: extreme bushfire. *Climatic Change*, 139(1).

Smith, I. et al. (2012) The relative performance of Australian CMIP5 models based on rainfall and ENSO metrics. *Australian Meteorological and Oceanographic Journal,* 63, pp.205-212.

Tawatsupa, B. et al. (2012) Heat stress, health and well-being: findings from a large national cohort of Thai adults. *BMJ open*, 2(6).

Taylor, K.A. et al. (2012): An Overview of CMIP5 and the Experiment Design. *Bulletin of the American Meteorological Society*, 93, pp.485-498.

Teague, B. et al. (2010) Final report, 2009 Victorian bushfires royal commission. Parliament of Victoria, Melbourne Victoria, Australia, 1.

Tian, Z. et al (2011) Experimental study on physiological and psychological effects of heat acclimatization in extreme hot environments. *Building and Environment*, 46(10), pp.2033-2041.

Tyson, P.D. & Preston-Whyte, R.A. (2000) The Weather and Climate of Southern Africa. 2nd ed., Oxford University Press, Cape Town; New York.

Virgilio, G. et al. (2019) Climate change increases the potential for extreme wildfires. *Geophysical Research Letters*, 46(14), pp.8517-8526.

Wang, S.-Y.S. and Yun, C.-ho (2017) Climate extremes: patterns and mechanisms. *Washington, D.C. Geophysical Monograph Series*, 226.

Worthy, M. and Wasson, R. (2004) Fire as an agent of geomorphic change in southeastern Australia: implications for water quality in the Australian Capital Territory. *Regolith, Canberra: CRC Landscape Environments and Mineral Exploration*, pp.417-418.

Zhao, T. and Dai, A. (2015) The Magnitude and Causes of Global Drought Changes in the Twenty-First Century under a Low–Moderate Emissions Scenario. *Journal of Climate, American Meteorological Society*, 28(11), pp.4490–4512.

Appendices

Appendix A

Appendix A includes three scatter plots of the change between historical (1980-2005) and future (2075-2100) simulations.

1. The change in the average relative anomaly Index of the High against the change in the frequency of extreme dry days.
2. The change in the average relative anomaly Index of the High against the change in the frequency of extreme heavy rainfall days.
3. The change in the average relative anomaly Index of the High against the change in the frequency of extreme high temperature days.

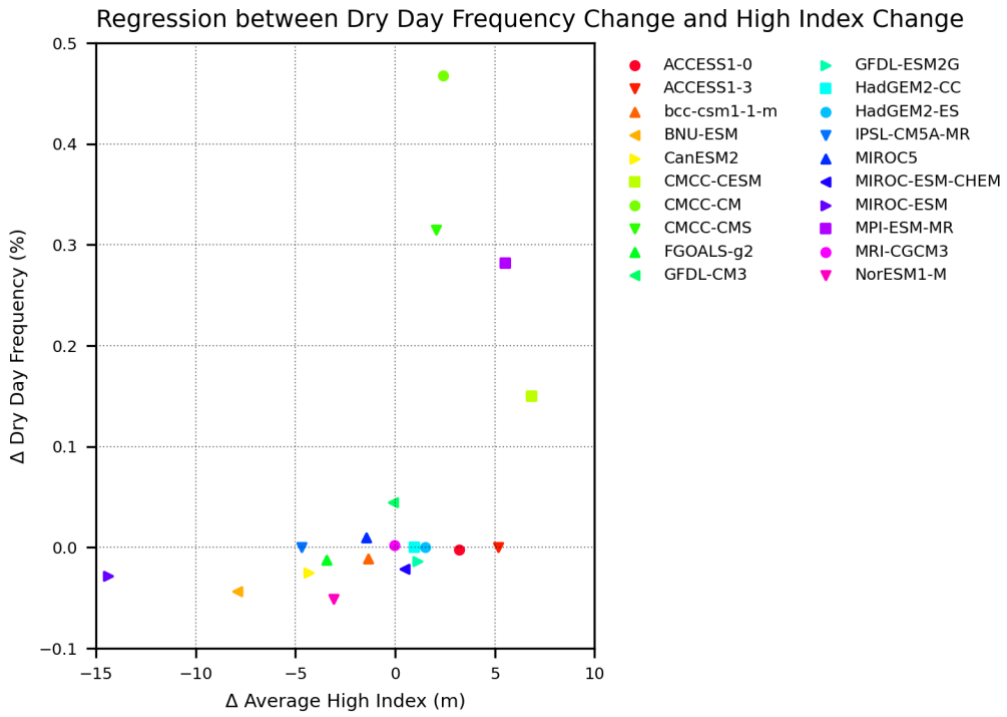

1.

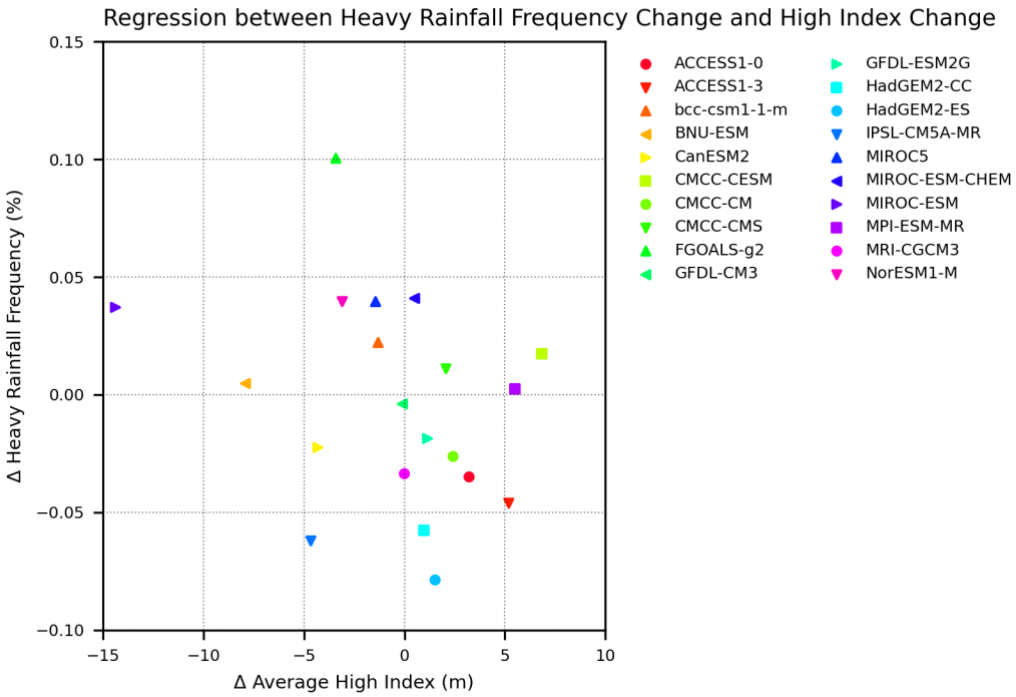

2.

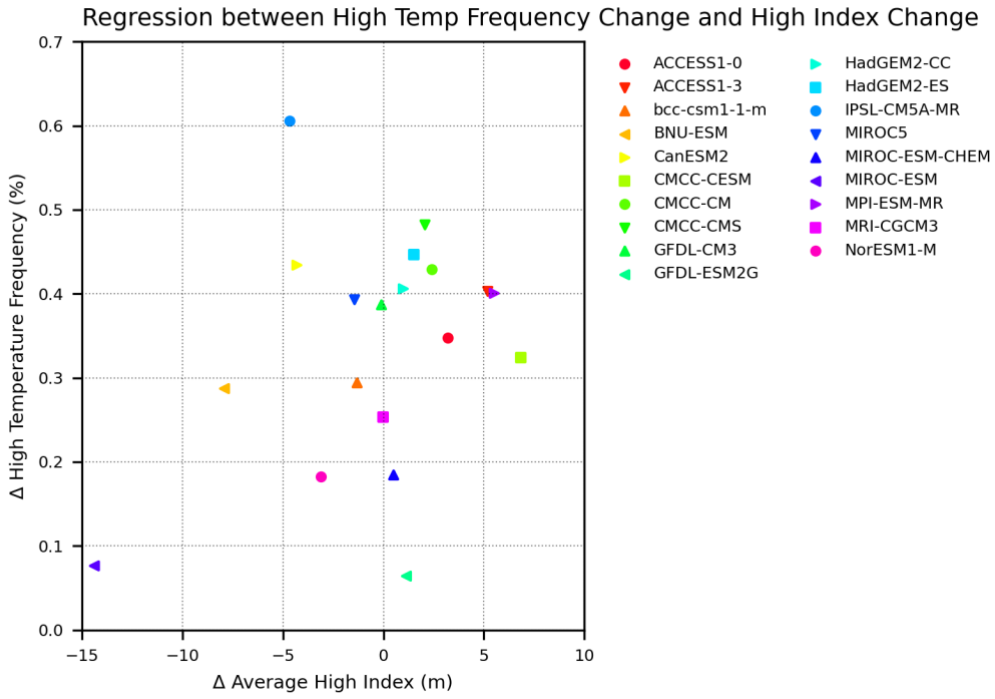

3.

Appendix B

Appendix B includes the following selection of the python scripts used to produce the plots presented in this dissertation. This does not contain all plots used within the dissertation but does show a representative selection of examples.

1. Script to create plot of Bilybara High Index (Figure 6)
2. Script to create plot of GPH composites using ERA5 data (Figure 7)
3. Script to create plot of Pearson's Correlation Coefficient between the High Index and temperature (Figure 10)
4. Script to create plot of anomaly composites of the relative frequency of extreme heavy rainfall days for 20 CMIP5 historical simulations (Figure 20)
5. Script to create scatter plot of the regression between rainfall change and High Index change between historical and future simulations (Figure 31)

Example 1: Bilybara High Index (Figure 6)

```
import numpy as np
import matplotlib.pyplot as plt
from matplotlib.ticker import MultipleLocator
from netCDF4 import Dataset
import calendar

# read netCDF file
f =
Dataset('../era5/gph_daily/standardised_anomaly_era5_daily_500gph_highcore_march_metres.1980
_2005.nc', mode='r')
timeseries = f.variables['z'][:,0,0]
f.close()

# set up figure
fig, ax = plt.subplots()

# create x axis
years = np.arange(len(timeseries))
years = (years / 31)

# plot wind profile
ax.plot(years, timeseries, color='orangered')

# add zero line
ax.plot(years, np.full(len(timeseries), 0), color='black')
```

```
# add title
ax.set_title('Bilybara High Index', fontsize=12)

# format x axis
ax.set_xlabel('Date')
ax.axes.set_xlim(0, 25)
ax.xaxis.set_major_locator(MultipleLocator(1))
ax.xaxis.set_minor_locator(MultipleLocator(1/15))

# format y axis
ax.set_ylabel('Standardised Anomaly')
ax.axes.set_ylim(-12, 10)
ax.yaxis.set_major_locator(MultipleLocator(1))
ax.yaxis.set_minor_locator(MultipleLocator(0.5))

# add gridlines
ax.grid(which='major', axis='both', linewidth=0.5, color='black', alpha=0.5, linestyle=':')

plt.xticks(np.arange(0, 26, 1))
labels = [item.get_text() for item in ax.get_xticklabels()]
labels[0] = '1980'
labels[1] = '1981'
labels[2] = '1982'
labels[3] = '1983'
labels[4] = '1984'
labels[5] = '1985'
labels[6] = '1986'
labels[7] = '1987'
labels[8] = '1988'
labels[9] = '1989'
labels[10] = '1990'
labels[11] = '1991'
labels[12] = '1992'
labels[13] = '1993'
labels[14] = '1994'
```

```
labels[15] = '1995'
labels[16] = '1996'
labels[17] = '1997'
labels[18] = '1998'
labels[19] = '1999'
labels[20] = '2000'
labels[21] = '2001'
labels[22] = '2002'
labels[23] = '2003'
labels[24] = '2004'
labels[25] = '2005'
ax.set_xticklabels(labels)
plt.xticks(rotation=45)

# make plot look nice
plt.tight_layout()

#plt.show()

# save figure to file
plt.savefig('../images/misc/daily_march_High_index_era5.png', orientation='portrait', format='png')

plt.close()
```

Example 2: GPH anomaly composite using ERA5 data (Figure 7)

```
import numpy as np
import matplotlib.pyplot as plt
import matplotlib.ticker as mticker
import cartopy.crs as ccrs
import sys as sys
from sys import exit
from netCDF4 import Dataset
from cartopy.mpl.gridliner import LONGITUDE_FORMATTER, LATITUDE_FORMATTER

# reading in high index values
```

```
f =
Dataset('../era5/gph_daily/standardised_anomaly_era5_daily_500gph_highcore_march_metres.1980
_2005.nc', mode='r')
array = f.variables['z'][:,0,0]
f.close()

# array = your 1d timeseries of anomalies
# find threshold for top 20% event - can select any percentile which makes sense #to you here....#
array_strong_threshold = np.percentile(array, 80)

# find indices above threshold
strong_indices = [i for i in range(len(array)) if array[i] > array_strong_threshold]



# array = your 1d timeseries of anomalies
# find threshold for top 20% event - can select any percentile which makes sense #to you here....#
array_weak_threshold = np.percentile(array, 20)

# find indices above threshold
weak_indices = [i for i in range(len(array)) if array[i] < array_weak_threshold]

# read in netCDF file for variable (gph/precip/temp)
ifile = '../era5/gph_daily/era5_daily_gph500_metres_Aus_march_1980_2005.nc'
f = Dataset(ifile, mode='r')
lons = f.variables['longitude'][:]
lats = f.variables['latitude'][:]
z = f.variables['z'][:,0,:,:]
# print(np.shape(z))
# exit()
f.close()

# open those indices in geopotential height/rain/temp 3d files ordered time/lat/lon
z_strong = z[strong_indices,:,:]

# to get average composite then do an average over the time dimension
z_strong_average = np.mean(z_strong, 0)
```

```
# open those indices in geopotential height/rain/temp 3d files ordered time/lat/lon
z_weak = z[weak_indices,:,:]

# to get average composite then do an average over the time dimension
z_weak_average = np.mean(z_weak, 0)

# create 2D fields of lons and lats
[lons2D, lats2D] = np.meshgrid(lons, lats)

# set up figure and map projection
fig, ax = plt.subplots(figsize=(5.5, 3.98), subplot_kw={'projection':ccrs.PlateCarree()})

# flatten axes object
#axflat = ax.flat

# define contour levels
levels = np.linspace(-100, 100, 51)

# contour data
mymap = ax.contourf(lons2D, lats2D, (z_strong_average - z_weak_average), levels,
transform=ccrs.PlateCarree(), cmap=plt.cm.bwr, extend='max')

# format map
ax.coastlines()
ax.set_extent([80, 175, -50, 10], crs=ccrs.PlateCarree())

# format gridlines and labels
gl = ax.gridlines(draw_labels=True, linewidth=0.5, color='black', alpha=0.5, linestyle=':')
gl.top_labels = False
gl.xlocator = mticker.FixedLocator(np.arange(-180, 180, 20))
gl.xformatter = LONGITUDE_FORMATTER
gl.xlabel_style = {'size':5, 'color':'black'}
gl.right_labels = False
gl.ylocator = mticker.FixedLocator(np.arange(-90, 90, 20))
gl.yformatter = LATITUDE_FORMATTER
```

```
gl.ylabel_style = {'size':5, 'color':'black'}

# add title
#ax.set_title('Geopotential Height Anomaly in March (using ERA5)', fontsize=12)

# add colorbar
cbarax = fig.add_axes([0.2, 0.07, 0.6, 0.02])
cbar = plt.colorbar(mymap, cax=cbarax, orientation='horizontal')
cbar.set_label('Geopotential Height [m]', rotation=0, fontsize=9, labelpad=1)
cbar.ax.tick_params(labelsize=5, length=0)

plt.tight_layout(h_pad=0, w_pad=-5, rect=[0,0.1,1,1])

#plt.show()

# save figure to file
plt.savefig('../images/era5/era5_strong_no_days_anomaly_march_gph500_composite.1980_2005.p
ng', format='png')

# close plot
```

Example 3: Pearson's Correlation Coefficient between the High Index and temperature (Figure 10)

```
import numpy as np
from scipy import stats
import matplotlib.pyplot as plt
import matplotlib.ticker as mticker
import cartopy.crs as ccrs
from netCDF4 import Dataset
from cartopy.mpl.gridliner import LONGITUDE_FORMATTER, LATITUDE_FORMATTER
from cartopy import feature
import pandas as pd

# reading in daily High index
```

```
ifile =
'../era5/gph_daily/standardised_anomaly_era5_daily_500gph_highcore_march_metres.1980_2005.n
c'
f = Dataset(ifile, mode='r')
array = f.variables['z'][:,0,0,0]
f.close()

# reading daily rainfall/temp data
ifile = '../era5/t2m_daily/era5_daily_t2m_Aus_march_1980_2005.nc'
f = Dataset(ifile, mode='r')
lons = f.variables['longitude'][:]
lats = f.variables['latitude'][:]
t2m = f.variables['t2m'][:,:,:]
t2m = t2m - 273.15
f.close()

# calculate correlation coefficients
rfield = np.zeros([len(lats), len(lons)])
pfield = np.zeros([len(lats), len(lons)])
#print(pfield)
#print(np.shape(array))
#print(np.shape(tp))

for y in np.arange(len(lats)):
    for x in np.arange(len(lons)):
        r, p = stats.pearsonr(array, t2m[:,y,x])
        rfield[y,x] = r
        pfield[y,x] = p
print('r range:', rfield.min(), rfield.max())
print('p range:', pfield.min(), pfield.max())

# create 2D fields of lons and lats
[lons2d, lats2d] = np.meshgrid(lons, lats)

# set up figure and map projection
fig, ax = plt.subplots(figsize=(5.5, 3.98), subplot_kw={'projection':ccrs.PlateCarree()})
```

```
# define contour levels
levels = np.linspace(-0.7, 0.7, 15)

# contour data
mymap = ax.contourf(lons2d, lats2d, rfield, levels, transform=ccrs.PlateCarree(),
cmap=plt.cm.PiYG, extend='neither')

# format map
ax.coastlines()
ax.set_extent([80, 175, -50, 10], crs=ccrs.PlateCarree())
# add colorbar
cbar = plt.colorbar(mymap, orientation='horizontal', shrink=0.7, pad=0.1)
cbar.set_label('Pearson\'s r', rotation=0, fontsize=10)
cbar.ax.tick_params(labelsize=7, length=0)

# add stippling for statistically significant domains
pfieldm = np.ma.masked_greater(pfield, 0.05)
ax.contourf(lons2d, lats2d, pfieldm, transform=ccrs.PlateCarree(), hatches=["..."], alpha=0.0)

# plot NINO3.4 domain
#ax.plot([-170, -120, -120, -170, -170], [-5, -5, 5, 5, -5], color='red', transform=ccrs.PlateCarree())

# add title
ax.set_title('Bilybara High Index and 2m Temperature Correlation', fontsize=10)

# make plot look nice
plt.tight_layout(pad=2.5)

#plt.show()
# save figure to file
plt.savefig('../images/era5/index_t2m_correlation_march_300dpi.png', format='png', dpi=300)
plt.close()
```

Example 4: Anomaly composites of the relative frequency of extreme heavy rainfall days for 20 CMIP5 historical simulations (Figure 20)

```
import sys as sys
from sys import exit
import numpy as np
import matplotlib.pyplot as plt
import matplotlib.ticker as mticker
import cartopy.crs as ccrs
from netCDF4 import Dataset
import numpy.ma as ma
import mpl_toolkits.basemap as bm
import scipy.stats.stats as stat
from cartopy.mpl.gridliner import LONGITUDE_FORMATTER, LATITUDE_FORMATTER
sys.path.append('/ouce-home/students/sedm5994/dissertation/')
#from outils import *

index_directory='../models/historical/gph/'
working_directory='../models/historical/pr/' #where your nc files are saved
savedir='../images/historical_models/Heavy_Rain/' #where you want the jpg saved

CMIP5_models=['ACCESS1-0', 'ACCESS1-3', 'bcc-csm1-1-m', 'BNU-ESM', 'CanESM2', 'CMCC-CESM', 'CMCC-CM', 'CMCC-CMS', 'FGOALS-g2', 'GFDL-CM3', 'GFDL-ESM2G', 'HadGEM2-CC', 'HadGEM2-ES', 'IPSL-CM5A-MR', 'MIROC5', 'MIROC-ESM', 'MIROC-ESM-CHEM', 'MPI-ESM-MR', 'MRI-CGCM3', 'NorESM1-M'] #list of models you want to plot
#wetyear_precip=[]
#CMIP5_models=['NorESM1-M']
for mm in CMIP5_models:

    f = Dataset(index_directory+mm+'standardised_anomaly_daily_500gph_highcore_March_metres.1980_2005.nc', mode='r')
    array = f.variables['zg'][:,0,0]
    f.close()

    # array = your 1d timeseries of anomalies
    # find threshold for top 20% event - can select any percentile which makes sense #to you here....#
    array_strong_threshold = np.percentile(array, 80)
```

```
    # find indices above threshold
    strong_indices = [i for i in range(len(array)) if array[i] > array_strong_threshold]
    # find threshold for top 20% event - can select any percentile which makes sense #to you here....#
    array_weak_threshold = np.percentile(array, 20)
    # find indices above threshold
    weak_indices = [i for i in range(len(array)) if array[i] < array_weak_threshold]

    e=Dataset(working_directory+mm+'.precip.1980-2005.MARCH.nc', mode='r') #read in your nc file - in this case precip
    pr=e.variables['pr'][:,:,:] #three dimensions; time; lat; longitude --> time is 0 here because assuming have already done a timemean in cdo
    lons=e.variables['lon'][:] #extracting lat and lon dimensions
    lats=e.variables['lat'][:]

    # open those indices in geopotential height/rain/temp 3d files ordered time/lat/lon
    pr_strong = pr[strong_indices,:,:]
    # open those indices in geopotential height/rain/temp 3d files ordered time/lat/lon
    pr_weak = pr[weak_indices,:,:]

    pr_new_strong = np.zeros(np.shape(pr_strong[0,:,:]))
    # find threshold for top 20% event - can select any percentile which makes sense #to you here....#
    pr_array_strong_threshold = np.percentile(pr_strong, 90)

    for lat in range(len(lats)):
        lat = int(lat)
        for lon in range(len(lons)):
            lon = int(lon)
            temp_counter = 0
            for i in range(len(pr_strong[:,lat,lon])):
                if pr_strong[i,lat,lon] > pr_array_strong_threshold:
                    temp_counter = temp_counter + 1
            pr_new_strong[lat,lon] = temp_counter/len(pr_strong[:,lat,lon])

    #print(np.shape(tp_new))
    pr_new_strong = pr_new_strong*100
```

```
    pr_new_weak = np.zeros(np.shape(pr_weak[0,:,:]))
    # find threshold for top 20% event - can select any percentile which makes sense #to you here....#
    pr_array_weak_threshold = np.percentile(pr_weak, 90)

    for lat in range(len(lats)):
        lat = int(lat)
        for lon in range(len(lons)):
            lon = int(lon)
            temp_counter = 0
            for i in range(len(pr_weak[:,lat,lon])):
                if pr_weak[i,lat,lon] > pr_array_weak_threshold:
                    temp_counter = temp_counter + 1
            pr_new_weak[lat,lon] = temp_counter/len(pr_weak[:,lat,lon])

    #print(np.shape(tp_new))
    pr_new_weak = pr_new_weak*100

    # create 2D fields of lons and lats
    [lons2D, lats2D] = np.meshgrid(lons, lats)

    # set up figure and map projection
    fig, ax = plt.subplots(figsize=(5.5, 3.98), subplot_kw={'projection':ccrs.PlateCarree()})

    # flatten axes object
    #axflat = ax.flat

    # define contour levels
    levels = np.linspace(-59, 59, 60)

    # contour data
    mymap = ax.contourf(lons2D, lats2D, (pr_new_strong - pr_new_weak), levels,
transform=ccrs.PlateCarree(), cmap=plt.cm.bwr, extend='max')

    # format map
    ax.coastlines()
    ax.set_extent([80, 175, -50, 10], crs=ccrs.PlateCarree())
```

```
    # format gridlines and labels
    gl = ax.gridlines(draw_labels=True, linewidth=0.5, color='black', alpha=0.5, linestyle=':')
    gl.top_labels = False
    gl.xlocator = mticker.FixedLocator(np.arange(-180, 180, 20))
    gl.xformatter = LONGITUDE_FORMATTER
    gl.xlabel_style = {'size':5, 'color':'black'}
    gl.right_labels = False
    gl.ylocator = mticker.FixedLocator(np.arange(-90, 90, 20))
    gl.yformatter = LATITUDE_FORMATTER
    gl.ylabel_style = {'size':5, 'color':'black'}

    # add title
    #ax.set_title('Heavy Rainfall Frequency in March (using '+mm+')', fontsize=12)
    ax.set_title("+mm+", fontsize=12)

    # add colorbar
    cbarax = fig.add_axes([0.2, 0.07, 0.6, 0.02])
    cbar = plt.colorbar(mymap, cax=cbarax, orientation='horizontal')
    cbar.set_label('Relative Frequency [%]', rotation=0, fontsize=9, labelpad=1)
    cbar.ax.tick_params(labelsize=5, length=0)

    plt.tight_layout(h_pad=0, w_pad=-5, rect=[0,0.1,1,0.9])

    #plt.show()
    # save figure to file

plt.savefig(savedir+mm+'_pr_models_extreme_heavy_precip_anomaly_march_composite.1980_20
05.png', format='png')
    # close plot
```

Example 5: Scatter plot of the regression between rainfall change and High Index change between historical and future simulations (Figure 31)

```
import numpy as np
import matplotlib.pyplot as plt
```

```
from netCDF4 import Dataset
from itertools import cycle
import scipy
import scipy.stats.stats as stat
from scipy.stats import pearsonr

working_directory='../models/historical/gph/'
second_working_directory='../models/rcp85/gph/'

# list of model names
modlist = ['ACCESS1-0', 'ACCESS1-3', 'bcc-csm1-1-m', 'BNU-ESM','CanESM2', 'CMCC-CESM','CMCC-CM', 'CMCC-CMS', 'FGOALS-g2','GFDL-CM3', 'GFDL-ESM2G', 'HadGEM2-CC', 'HadGEM2-ES', 'IPSL-CM5A-MR','MIROC5', 'MIROC-ESM-CHEM','MIROC-ESM', 'MPI-ESM-MR', 'MRI-CGCM3','NorESM1-M']

# set up figure and map projection
fig, ax = plt.subplots(figsize=(5.5, 3.98))

# set up sequences of colours and symbols
colors = iter(plt.cm.gist_rainbow(np.linspace(0, 1, len(modlist))))
cycle_marker = cycle(['o', 'v', '^', '<', '>', 's'])

gph = []
rainfall = []

# loop through models
for i, m in enumerate(modlist):
    # read two model files (pr and tas)
    f = Dataset('../models/anomalies/'+m+'_anom_pr.nc', mode='r')
    pr = f.variables['pr'][:,0,0]
    pr = pr *86400
    f.close()
    # reading in high index values
    f=Dataset(working_directory+m+'.gph_relative_anom.1980-2005.MARCH_timmean.nc',
mode='r')
    array1 = f.variables['zg'][:,0,0]
```

```
    f.close()
    # reading in high index values
    f=Dataset(second_working_directory+m+'.gph_relative_anom.2075-2100.MARCH_timmean.nc',
mode='r')
    array2 = f.variables['zg'][:,0,0]
    f.close()

    # scatter data
    ax.scatter((array2 - array1), pr, c=next(colors), marker=next(cycle_marker), s=10, label=m)

    gph.append(array2 - array1)
    rainfall.append(pr)

# format x-axis
ax.set_xlim(-15, 10)
ax.set_xlabel('\u0394 Average Relative Anomaly High Index', fontsize=7)

# format y-axis
ax.set_ylim(-2.5, 2.5)
ax.set_ylabel('\u0394 Precipitation [mm day$\mathregular{^{-1}}$]', fontsize=7)

# formats for both axes
ax.tick_params(axis='both', which='major', labelsize=6)
ax.grid(linewidth=0.5, color='black', alpha=0.5, linestyle=':')

# add legend
plt.subplots_adjust(right=0.6)
ax.legend(loc='upper left', bbox_to_anchor= (1.02, 1.0), fontsize= 6, ncol=2, frameon=False)

# add title
ax.set_title('Regression between Rainfall Change and High Index Change', fontsize=12)

gph_as_array=np.array(gph, dtype='float')
rainfall_as_array=np.array(rainfall, dtype='float')

#plt.show()
```

```
# save figure to file
#plt.savefig('../images/anom_gph_pr_scatter_300dpi.png', format='png',dpi=300)
# close plot
plt.close()
```